CHALMERS

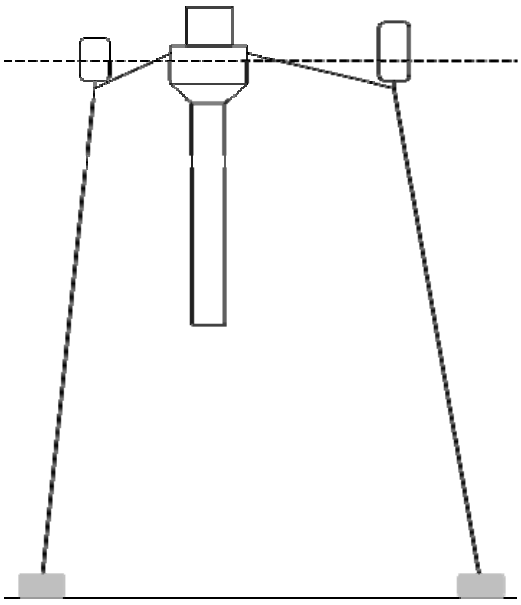

Mooring of a wave power device

Simulation of the dynamic response to wave loading

Master of Science Thesis in the Master's Programme Solid and Fluid Mechanics

JOHANNES PALM

Department of Civil and Environmental Engineering
Division of Water Environment Technology

CHALMERS UNIVERSITY OF TECHNOLOGY
Göteborg, Sweden 2010

Master's Thesis 2010:105

MASTER'S THESIS 2010:105

Mooring of a wave power device

Simulation of the dynamic response to wave loading

Master of Science Thesis in the Master's Programme Solid and Fluid Mechanics

JOHANNES PALM

Department of Civil and Environmental Engineering
Division of Water Environment Technology

CHALMERS UNIVERSITY OF TECHNOLOGY
Göteborg, Sweden 2010

Mooring of a wave power device

Simulation of the dynamic response to wave loading

Master of Science Thesis in the Master's Programme Solid and Fluid Mechanics

JOHANNES PALM

Examensarbete / Institutionen för bygg- och miljöteknik,
Chalmers tekniska högskola 2010:105

Department of Civil and Environmental Engineering

Division of Water Environment Technology

Chalmers University of Technology

SE-412 96 Göteborg

Sweden

Telephone: + 46 (0)31-772 1000

Reproservice, Chalmers tekniska högskola, Göteborg, Sweden 2010

Mooring of a wave power device

Simulation of the dynamic response to wave loading

Master of Science Thesis in the Master's Programme Solid and Fluid Mechanics

JOHANNES PALM

Department of Civil and Environmental Engineering

Division of Water Environment Technology

Chalmers University of Technology

ABSTRACT

A wave power device can have many different forms. This thesis focuses on the problem of mooring the WaveEl buoy, a self-reacting, floating wave power device. The mooring system is composed of three floaters surrounding the buoy. Each floater is connected to the buoy by a horizontal line, and each floater is moored to the seabed by a vertical line. The mooring line is a fibre line which is highly elastic.

The problem of mooring a wave power device is that the mooring system should allow the buoy to move freely in the vertical direction, but at the same time restrain the horizontal motion. The mooring system of the WaveEl buoy has been the focus of this thesis and its performance in different load conditions has been studied. The Finite Element Method has been implemented in a MATLAB program for the dynamic analysis of the response to wave loading in the mooring lines. In this process also the motion of the buoy is studied, as it is the most essential component in determining the mooring forces.

Results show that the WaveEl buoy has a dynamic range in heave between period times of $T = 2.25\,s$ and $T = 4.25\,s$ of the waves. This is suitable as the most common waves in the area of operation are of period times around $T = 4\,s$. The vertical motion amplitude relative the wave amplitude in single frequency loading varies from 0.45 for resonance with free piston, up to 1.8 at resonance for the locked piston position. The buoy motion is strongly affected by sea current conditions, but also by the amount of pre-tension in the mooring lines. With increased pre-tension, the system responds more rigidly and the horizontal offset due to current loading is decreased. However, with increased pre-tension, the floaters are more submerged and the dissipation of energy of the mooring system increases.

The mooring forces are highly dependent on the slacking and re-tightening of the line and it in this process that the maximum forces are obtained. The system is supposed to remain taut at all times and to avoid this in the future an increased floater size is possible.

Key words: Moorings, Wave Power, Taut elastic lines, Resonance frequency, Wave loading

Förankring av ett vågkraftverk

Simulering av den dynamiska responsen på grund av våglaster

Examensarbete inom Mechanics of Solids and Fluids

JOHANNES PALM

Institutionen för bygg- och miljöteknik

Avdelningen för Vatten Miljö Teknik

Chalmers tekniska högskola

SAMMANFATTNING

Vågkraftverk kan ha en rad olika former och utseenden. Denna uppsats fokuserar på problemet att förankra WaveEl bojen: ett flytande, själv-reagerande vågkraftverk. Förankringslösningen består av tre flottörer som är utplacerade runt omkring bojen. Dessa tre är förbundna med bojen via elastiska fiberlinor. Varje flottör är i sin tur fastsatt i ankare på havsbottnen via ytterligare en lina. Problemet med att förankra ett vågkraftverk av denna typ är att man vill förhindra all horisontell rörelse utan att för den delen bromsa den vertikala rörelsen på något sätt.

Syftet med uppsatsen har varit att utvärdera WaveElbojens förankringssystem genom att bygga upp en MATLAB modell av den dynamiska responsen från vågkrafter. Denna analys har använt sig av Finita Element Metoden för att beskriva förankringskrafterna i linorna. Förankringskrafterna är programmets viktigaste utdata, men även bojens rörelser studeras.

Resultaten visar att WaveEl-bojens resonansperioder varierar mellan 2.25 s och 4.25 s beroende på om kolven är låst eller fri att röra sig relativt bojen. Dessa resultat passar bra gentemot de vanligaste våglängderna i området som har en periodtid på runt 4 s. Bojens vertikala rörelseamplitud relativt amplituden på inkommande våg varierar från 0.45 till 1.8 för fri respektive låst kolv. Bojens jämviktsposition i horisontalled är starkt beroende av havsströmmens styrka och rikting, men också av hur förspända linorna är i jämviktsläget. Med en ökad förspänning i linorna så minskar den horisontella avdriften.

Förankringssystemet klarar i dagsläget inte riktigt av att hålla sig spänt hela tiden, utan perioder av slak lina förekommer ofta i de horisontella linorna. Detta är något som bör undvikas och därför kan det bli aktuellt att undersöka effekten av större flottörer och ett hårdare spänt system.

Nyckelord: Vågkraftverk, Förankring, Spänt, elastiskt linsystem, Resonansfrekvens, Vågkrafter

Contents

Preface

This paper has been the last examination of my education at Chalmers University of Technology. There are many things that one can take into account when looking into Wave Power and its many uses and challenges. For me it has offered an ideal opportunity to learn about simulations in aquatic environments and to work with renewable sources of energy. This has been a technical project and nothing about the economic or environmental aspects of the WaveEl project has been taken into account. Of course some simplifications and approximations have been made in the modelling, as I have built the computer model from scratch, but in general most forces acting on partly submerged structures have been taken into account.

The mooring of a wave power device is more complicated than it first may seem and especially the large displacements give rise to large tension forces in the mooring lines. From a technical point of view there are some changes that can or need to be made before the mooring system solution is mature enough to be used commercially. The basic geometrical solution is however very good and most of the changes involve alteration of the dimensions of different parts of the system.

When it comes to the mooring system, the WaveEl buoy is tautly moored, whilst all other floating wave power devices are slack-moored, and this enables a possibility for position mooring. If one could find a good way to keep the buoy relatively stationary in the horizontal direction, a wave power park of buoys can have a much higher density of wave power devices than others and I truly hope that I will be able to continue to work with this on some level, and that the WaveEl project will be successful.

Göteborg June 2010

Johannes Palm

Notations

F.E. system notations

$\boldsymbol{F}$	Load vector
$\boldsymbol{g}$	Error function of the free degrees of freedom.
$\boldsymbol{J}$	Jacobian matrix.
$\boldsymbol{K}$	Assembled stiffness matrix of the system
$\boldsymbol{M}$	Assembled mass matrix of the system.
$\boldsymbol{r}$	Position vector of all degrees of freedom.

Notations concerning the buoy

$\boldsymbol{A}$	3 by 3 matrix for added mass
b_x	Radiation damping coefficient in surge.
b_z	Radiation damping coefficient in heave.
$\boldsymbol{B}$	3 by 3 matrix for radiation damping
c_z	Hydrodynamic restoring coefficient in heave.
C	3 by 3 matrix for hydrodynamic restoring coefficients.
$\boldsymbol{F}_B$	Buoyancy force vector
$\boldsymbol{F}_D$	Drag force vector
$\boldsymbol{F}_{Mi}$	Mooring force vector number i acting on the buoy
$\boldsymbol{I}$	Moment of inertia of the buoy about its center of mass.
$\boldsymbol{I}_a$	Added moment of inertia of the buoy due to added mass.
$\boldsymbol{R}_{rot}$	3 by 3 rotation matrix from global to local coordinate system
V	Submerged volume of buoy.
$\boldsymbol{\eta}$	Translational displacement vector of the buoy in m.
$\boldsymbol{\phi}$	Rotational displacement vector of the buoy in rad.
ω_0	Natural- or eigenfrequency of the buoy in Hz.

Mooring system and geometry notations

A	Cross-sectional area of mooring line.
dL	Length of mooring line element.
F_i	Tension force in line number i.
H	Water depth.
$K(\epsilon)$	Elasticity of the mooring line per unit length.
L_i	Length of mooring line number i.
α_i	Angle between horizontal plane and line number i.
γ	Mass per unit length of mooring line.
γ_a	Added mass per unit length of mooring line.
γ_e	Effective mass per unit length of mooring line.
ϵ_i	Strain in line number i.
φ_i	Angle between vertical axis and line number i.
ϕ_1	Basis function for node 1 of mooring line element.
ϕ_2	Basis function for node 2 of mooring line element.

Wave and sea current notations

a	Wave amplitude
$D(\theta)$	Directionality distribution of irregular wave.
k	The wave number of the wave, $k = \frac{2\pi}{\lambda}$.
$S_J(\omega)$	JONSWAP spectrum of irregular wave.
T	Wave period
u	Horizontal velocity of water particles in wave motion.
$\boldsymbol{v}_c$	Velocity of sea water current.
$\boldsymbol{v}_w$	Velocity of water particles.
w	Vertical velocity of water particles in wave motion.
ζ_i	Phase shift of wave component i in irregular waves.

θ_c Angle between x-axis and the direction the water current.

θ_w Angle between x-axis and the direction of propagation of the wave.

$\hat{\boldsymbol{\kappa}}$ Direction of propagation of wave.

λ The wavelength.

ξ_κ Horizontal displacement of water particles in wave motion.

ξ_z Vertical displacement of water particles in wave motion.

Φ Velocity potential of the wave.

ω Wave frequency

General notations

C_{Di} Drag coefficient of type i.

d Diameter

m_{ai} Added mass in direction i.

r Radius.

Re Reynolds number of the water loading scenario.

t Time of simulation.

$\hat{\boldsymbol{t}}$ Tangential unit vector of the body.

T_{end} Maximum simulation time.

$\boldsymbol{v}_{body}$ Velocity of body.

$\boldsymbol{v}_{rel}$ Relative velocity between water and body.

α Time integration variable in Newmark method.

β Fraction of body that is submerged in water.

δ Time integration variable in Newmark method.

Δt Time step size.

ν Kinematic viscosity of sea water.

ρ_{line} Density of mooring line, kg/m^3.

ρ_w Density of sea water, kg/m^3.

1 Introduction

The primary objective of this master's thesis has been to create a model that enables a three dimensional dynamic analysis of the mooring system of the WaveEl wave power buoy. To do this the interaction between the wave- and current-induced motion of the water and all parts of the mooring system, as well as the buoy itself, has been taken into account. All simulations have been performed in MATLAB and all used scripts and subroutines have been written for this particular purpose during the course of the thesis.

1.1 The WaveEl project

The WaveEl project is a cooperation between Reinertsen, Göteborg Energi, Frog Construction and Diving AB, and Bohegg Engineering.

The WaveEl is a wave power device that can be classified as a self-reacting point absorber. A prototype has been developed and is currently in operation outside of Vinga in the Gothenburg archipelago. The prototype is equipped with measuring instruments that have been specifically placed for evaluation of the power generation and the performance of the mooring system. It is generating power, but it is not producing it to the power grid as yet. The WaveEl project involves different areas of research, and it is in the simulation of the mooring forces that this thesis comes into play. As many of the problems occurring are new, there is much to gain in the building of a computer model to study the forces in the mooring lines and the motion of the buoy. In order to properly evaluate the buoy prototype, it is of interest to make a systematic analysis of the different factors affecting the system to see how it responds. The primary purpose of this thesis has thus been to build a computer model of the mooring system using MATLAB and the Finite Element Method, and to use this to study the behaviour of the WaveEl buoy.

1.2 Wave power and mooring

Wave power is by no means a new invention. Its primary time of development was during the oil crisis in the 1970's. During the last ten years there have been many new projects, and there are now a number of different types of wave power devices, both old and new, in operation. The WaveEl buoy is originally based on a project from the 1970's but much of the technology has been upgraded. The buoy is an example of a self-reacting device, which puts extra demands on the mooring system. The following section discusses the mooring techniques of other wave power devices of self-reacting character.

1.2.1 Mooring systems of self reacting devices

A self-reacting device is not rigidly fastened to the seabed and does not rely on the seabed to create the reaction force needed to generate energy. Instead one can define it as a device that has two parts with different hydrodynamic properties that are allowed to move in relation to each another. The relative motion can, by means of any of the different techniques available, be used to absorb energy from the motion of the waves. There are two main categories of self-reacting devices; axi-symmetric and directional. Axi-symmetric devices are point-absorbers and have the general form of a buoy moving up and down in the waves, whilst the appearance of a directional device can be very diverse and is most easily described for each case.

The demands on a mooring system for a wave power device are extremely dependent on the form of device, and its means of generating power. In general the mooring needs to be able to sustain a lot of load, to ensure that the device does not come loose in heavy sea, but it must also ensure that it does not restrain the movement of the device in such a way as to induce dissipation of energy.

Another general system requirement concerns the position mooring required in a wave power park. If the device shall be placed in a matrix of devices it is essential that the horizontal motion is restrained in such a way as to enable a desired spacing between the devices. Depending on the type of device, there is an optimal spacing that ensures the best power output of the whole system, according to Fitzgerald (2009), and this spacing is in general smaller than the horizontal area needed for one device using conventional mooring techniques.

Here follows an account of a few contemporary solutions for wave power generation that are under development; and special attention is of course paid to the mooring system of each device.

1.2.1.1 The Pelamis

The Pelamis is the leading solution in wave power when it comes to meeting cost and power output demands. The next generation, the Pelamis P2, is planned to be installed outside the Shetland Islands and start producing 20MW of power in 2014. The project is a partnership between Vattenfall and Pelamis ltd.

The Pelamis has the form of a long, snake-like device, see Figure 1.1, that uses hydraulic hinges between its different sections and the pressure generated there to drive hydraulic motors, which in turn drive generators. Power is transmitted to a junction at the seabed and from there to shore through an underwater cable. This junction serves as a hub and can be used to connect several devices. This is done to decrease the installation cost of larger wave power parks or farms.

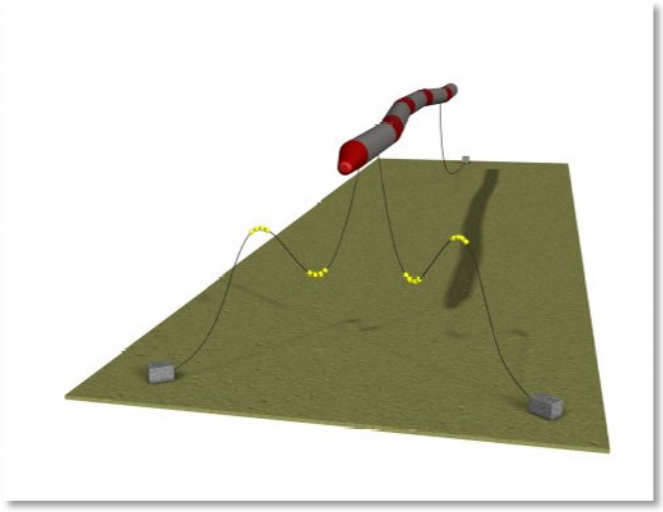

Figure 1.1: The mooring system of the Pelamis device; two lines at the front and one at the rear.

The mooring system, shown in Figure 1.1, is composed of three mooring legs; two at the front and one at the rear. All of the legs are slack-moored, but the two front legs include a floater and a sinker. As these two are separated by a certain distance, it means that the line basically works as a spring with a restoring force, caused by gravity acting on the sinker and the lifting force of the floater, which both act to restore equilibrium. In this way it gives the mooring leg, which for instance may be composed of an inelastic chain, a geometric elasticity that enables the Pelamis to move and turn in response to the waves.

Such flexibility is essential to the functionality of the power station as it is built in such a way as to be most efficient when facing the waves. Thus one of the most important mooring criteria is that the Pelamis must be allowed to rotate at least 180 degrees about its midpoint.

The Pelamis is a typical example of a directional device. A key feature is that as it uses the relative angular momentum of its different parts to generate power, the system is less sensitive to constraints from the mooring system. However it does have a large span and either of the front lines or the rear line will be subjected to large forces, depending on wind magnitude and speed. The large spacing required to avoid entanglement in a slack-moored wave power park is the major drawback of the slack-moored solution. Another issue is the dissipation, or loss, of energy due to mooring system constraints.

1.2.1.2 The Wave Dragon

The Wave Dragon is an example of an off-shore overtopping device. This floating platform is designed to let the wave crests top over the edges into a reservoir. The water then passes through turbines on its way back down from the reservoir into the sea. One of the key features of the Wave Dragon is that it uses well developed water power turbines in their generators and so can make good use of conventional technology. Figure 1.2 shows that the platform is very large and that it is moored so

that it can rotate freely about a relatively fixed buoy. This however takes up a large area, and Figure 1.2 also shows the probable dimensions of an array of Wave Dragons.

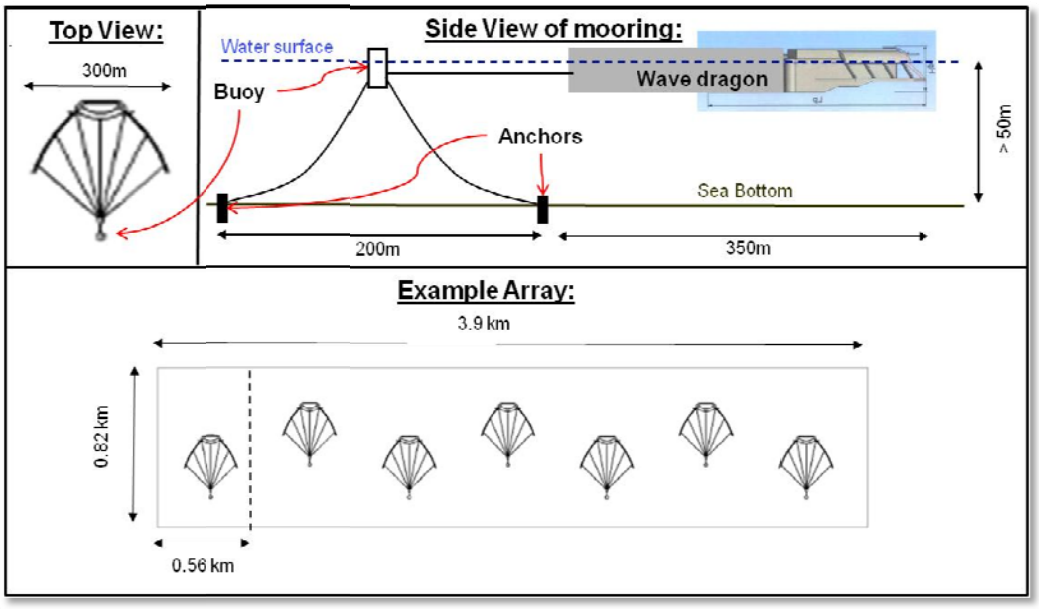

Figure 1.2: Wave dragon mooring system and the dimensions of an array of 7 MW devices. Figure from personal correspondence with Wave Dragon (2010)

A 7 MW device is moored with 6 to 8 mooring lines according to the Wave Dragon project group (2010). This is how the buoy remains relatively stationary even in rough seas, which enables the array to be as tightly planned as it is. The advantage of this type of mooring system is that the dragon can swivel around the buoy, thus enabling it to align with the other dragons and to face the wave direction. This is essential as it is designed to face the waves from one direction, and it is therefore also an example of a directional device.

This type of mooring also has the advantage of not restricting the vertical motion of the dragon, as the force exerted on the Wave Dragon by the mooring line to the buoy is basically horizontal, due to its length. The disadvantage is that it takes up a lot of space. This need of the Wave Dragon to swivel around and face the wave front is decisive when evaluating mooring possibilities.

1.2.1.3 The Wavebob

A third example is the Wavebob. It is a point absorber and is, when it comes to the design, the closest to the WaveEl buoy today.

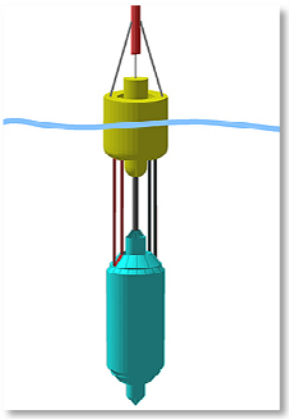

Figure 1.3: The schematics of the self-reacting device Wavebob. www.wavebob.com

The Wavebob homepage states that the Wavebob will be slack-moored, but no further information is given. In the contact with one of their collaborators, Vattenfall, it has become evident that not all mooring problems have yet been solved, and it is therefore a reasonable assumption that other mooring possibilities might be taken under consideration.

1.3 Problem description

The WaveEl buoy is moored by a system of elastic fibre mooring lines that are very strong in tensile loading, but very weak in bending and compression. The elasticity of the lines makes it possible to have a taut system of lines, and in this way keep the buoy relatively stationary. The geometry can be seen in Figure 1.4.

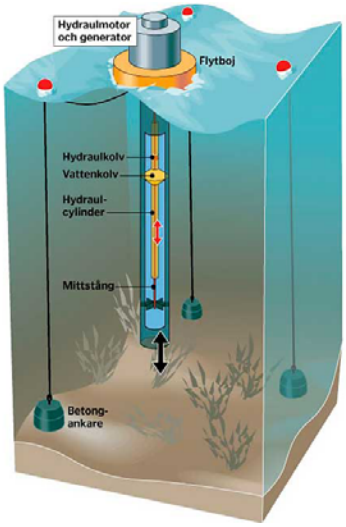

Figure 1.4: A schematic figure of the buoy and the mooring system. One of the three floaters is in reality larger than the two others, and the horizontal mooring lines are taut and not slack. The figure is taken from www.nyteknik.se/nyheter/energi_miljo/energi/article553532.ece

The three floaters that surround the buoy are each connected to two mooring lines; one vertical mooring it to the gravity anchor at the seabed, and one horizontal attaching it to the buoy. It is the dynamics of this system that have been investigated in this thesis. The choice was made to write a MATLAB based FEM- program to solve this, as the nature of the interaction between the structure and the water is so complex and non-linear. Initial attempts were made to simulate it in ADINA, but many terms in the equations would have been very difficult to simulate without the use of a more specific modelling program. The primary output of the program is the tension in the mooring lines, and their maximum value in different loading scenarios, but also the motion of the buoy due to the incoming waves and the effect of sea water current are studied. In order to properly simulate the interaction between the structures and the fluid, there are a number of things to consider, which are briefly described in the following chapter.

2 Theory

2.1 Bodies submerged in water

All geometry in this thesis is of cylindrical type, and the following theoretical descriptions are therefore restricted to this geometrical setting.

2.1.1 Hydrodynamic mass

When a body moves in water, it does not only accelerate its own mass, but also some of the surrounding water. The mass of this affected surrounding body of water, is referred to as the hydrodynamic mass, or added mass, of the body. It is of course highly dependent on the geometry, as well as the direction of the motion. It is also, in a wave loading scenario, dependent on the frequency of the exiting wave motion. The frequency dependence is however not taken into consideration in this thesis. When it comes to cylindrical bodies there are two different added volumes, one for the sides and one for the top and bottom of the cylinder. The situation is described by Figure 2.1 below.

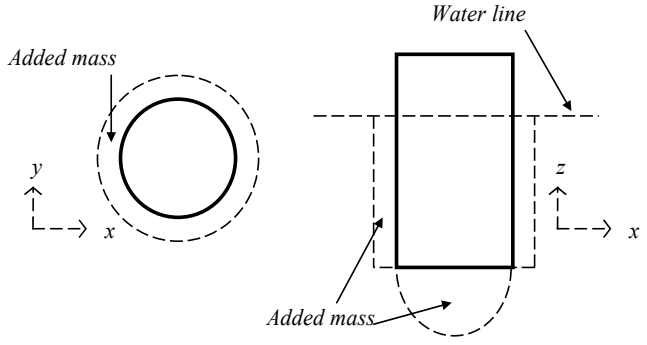

Figure 2.1: A schematic drawing of the added mass of a cylinder semi-submerged in water.

Mathematically the extra cylinder of the sides has the same volume as the inner cylinder, i.e. the body itself, and the added volume at the bottom is about 60% of the volume of a half-sphere of the same radius as the body, so that $m_a = C_m\, \rho_w \frac{2}{3}\, \pi r^3$ where $C_m = 0.64$ is the coefficient of added mass taken from D.N.V (2000). Thus, for a fully submerged cylinder of length L and radius r, the following expressions decide the added masses of the different directions of motion:

$$m_{ax} = m_{ay} = \rho_w L\, \pi r^2 \qquad (2.1)$$

$$m_{az} = 0.64\, \rho_w \frac{4}{3}\, \pi r^3 \qquad (2.2)$$

In heave, that is vertical motion the term m_{az} is used to describe the added mass, and in surge or sway, that is in horizontal motion, m_{ax} and m_{ay} are used instead. The

added mass has one property that sets it apart from the mass of the body. The added inertia force is proportional to the relative acceleration between body and water, whilst the normal inertia force depends on the absolute acceleration of the body alone.

2.1.2 Drag forces

The drag force is basically the friction force acting on a body moving in any viscous fluid. When a body gathers velocity in water it will be subjected to a drag force per unit length which can be expressed as:

$$\boldsymbol{F}_D = \frac{C_D \rho_w}{2} |\boldsymbol{v}_{rel}| \, \boldsymbol{v}_{rel} \tag{2.3}$$

Here C_D is the drag coefficient which depends on the shape of the body, the roughness of its surface and the maximum speed of the water particles. The force is proportional to the effective area that is exposed to the relative velocity and is directed in the same direction as the relative velocity. In this thesis there are two separate geometrical types that are subjected to drag forces: the mooring line elements where the effect of the top and bottom of the cylinder can be neglected, and the buoy and the floaters where the top and bottom must be considered. The drag force coefficient is naturally much smaller in the tangential direction of the body than it is in the normal, transverse direction, and is therefore not included in (2.4). Thus the effective drag coefficients of the sides and the bottom or lid of a cylinder submerged in water can be expressed as follows, where d is the diameter of the body.

$$\begin{aligned} C_{Dside} &= C_{DCyl}\, d \\ C_{Dlid} &= C_{DPlate}\, \pi \frac{d^2}{4} \end{aligned} \tag{2.4}$$

In the case of the mooring line C_{Dlid} is not used. The drag force is given per unit length and $\boldsymbol{v}_{rel}$ in (2.3) is the relative velocity between the water and the body.

$$\boldsymbol{v}_{rel} = \boldsymbol{v}_w - \boldsymbol{v}_{body} \tag{2.5}$$

This means that the constant C_D in (2.3) is a function of the direction of the relative velocity, and the equation is split into the tangential and the transverse direction of the body.

The approximation of the numerical values of C_D for the different bodies is described in Section 3.3.1.

2.2 Wave theory

The waves used in the simulations of this thesis are based on linear wave theory with the use of the velocity potential,Φ, as a solution to Laplace's equation. The linearized boundary value problem is defined in equation (2.6) below.

$$\frac{\partial^2 \Phi}{\partial \mathrm{x}^2} + \frac{\partial^2 \Phi}{\partial \mathrm{y}^2} + \frac{\partial^2 \Phi}{\partial \mathrm{z}^2} = 0$$

$$\left.\frac{\partial^2 \Phi}{\partial \mathrm{t}^2}\right|_{z=0} + g \left.\frac{\partial \Phi}{\partial \mathrm{z}}\right|_{z=0} = 0 \qquad (2.6)$$

$$\left.\frac{\partial \Phi}{\partial \mathrm{z}}\right|_{z=-H} = 0$$

The velocity potential, Φ, is here a solution to Laplace's equation with the use of the free surface boundary condition and that the vertical motion of the water particles at the seabed is nil. With this in mind, the following expression for the velocity potential is used in the simulations.

$$\Phi = -\frac{a\, g}{\omega} \frac{\cosh\big(k(H+z)\big)}{\cosh(kH)} \cos\left(k\kappa - \omega t\right) \qquad (2.7)$$

Here H is the water depth, a is the amplitude of the wave and κ is the coordinate along the wave propagation direction starting from the origin of the xy-plane. For a wave travelling along the x-axis, $\kappa = x$ and for a wave along the negative y-axis, $\kappa = -y$. $\hat{\boldsymbol{\kappa}}$ is thus the unit vector pointing in the direction of propagation of the two dimensional plane wave, and will always be in the xy-plane. This means that the wave properties must be translated into the global x- and y-system before the forces can be applied. All wave properties can be derived from (2.7) using the following relations.

$$\mathrm{u} = \frac{\partial \Phi}{\partial \kappa} \qquad (2.8)$$

$$\mathrm{w} = \frac{\partial \Phi}{\partial \mathrm{z}} \qquad (2.9)$$

$$\xi_\kappa = \int_0^t \frac{\partial \Phi}{\partial \kappa}\, d\tau \qquad (2.10)$$

$$\xi_z = \int_0^t \frac{\partial \Phi}{\partial \mathrm{z}}\, d\tau \qquad (2.11)$$

$$P_d = -\rho_w \frac{\partial \Phi}{\partial \mathrm{t}} \qquad (2.12)$$

Where u and w are the horizontal and vertical velocities and, ξ_κ and ξ_z are the particle paths of the water. P_d is the dynamic pressure of the water. The accelerations are obtained from derivation of u and w with respect to time. For a more complete theoretical derivation of the equations, see Bergdahl (2009).

2.3 Wave loading

This section includes a brief description of the forces acting on a submerged or partly submerged body in an accelerated fluid. The governing equations of this section are under the assumption that Morison's formula is valid, see Bergdahl (1979). The forces on a body according to Morison can be expressed by the relative velocity and acceleration between the body and the water and the approximation is valid for small objects. A general criteria is that $4d \leq \lambda$, where λ is the wavelength of the wave and d is the diameter of the body. The forces are a superposition of restoring reaction forces due to the displacement of the body from its equilibrium position, and the exciting wave forces. In the case of a vertical cylinder in translational motion, the equations differ between the heave and the surge (or sway) equations. The surge and sway equations are equivalent in this case, due to the cylindrical shape.

Let $\boldsymbol{\xi} = \left[\xi_x\ \xi_y\ \xi_z\right]^T$ be the vector describing the water particle positions in the undisturbed wave, and $\boldsymbol{\eta} = \left[\eta_x\ \eta_y\ \eta_z\right]^T$ the translational displacement of the buoy from its equilibrium position. Forces come from the pressure gradient across the body, viscous damping drag forces and the inertia force due to the acceleration of the body and its added mass. When the buoy is operating it is also exerting a damping force proportional to the relative velocity. To these forces one must add reaction forces from the water that work as primary restoring forces and also the radiation damping that comes from that the body moving at the surface will radiate waves and thereby dissipate energy.

Heave: $$(m_z + m_{az})\ddot{\eta}_\mathrm{z} = m_{az}\ddot{\xi}_z + b_z\left(\dot{\xi}_z - \dot{\eta}_z\right) - c_z\eta_z + P_d + F_{Mz} + F_{Dz} \qquad (2.13)$$

Surge: $$(m_x + m_{ax})\ddot{\eta}_\mathrm{x} = (\rho_w V + m_{ax})\ddot{\xi}_x + b_x\left(\dot{\xi}_x - \dot{\eta}_x\right) + F_{Mx} + F_{Dx} \qquad (2.14)$$

The force from the dynamic pressure gradient acting on the bottom area of the body is here represented by P_d. In the surge/sway equation the Froude-Krylov force $\rho_w V\ddot{\xi}_x$ where V is the volume, is present, which for small bodies (in relation to the

wavelength) can be said to be equivalent to the effect of the pressure gradient. b_x and b_z are the coefficients of radiation damping, c_z is the hydrodynamic restoring coefficient, and F_D and F_M are the drag and mooring forces.

Equations (2.13) and (2.14) represent the translational motion of the buoy, but it is also subjected to moments and is allowed to rotate. Let now $\boldsymbol{\phi} = \left[\phi_x\ \phi_y\ \phi_z\right]^T$ be the angular displacement about the local x-, y- and z-axis of the buoy. Let also $\boldsymbol{r}_B$ and $\boldsymbol{r}_{Mi}$ denote the vector from the centre of mass to the buoyancy point and the mooring point number i respectively, in the local coordinate system. $\boldsymbol{F}_B$ is the buoyancy force. Then the moment equation of the buoy is written as

$$(\boldsymbol{I} + \boldsymbol{I}_a)\ddot{\boldsymbol{\phi}} = \int_l \mu \times \boldsymbol{R}_{rot}\left[\boldsymbol{F}_D(\mu) + (\rho_w \boldsymbol{V} + \boldsymbol{A})\ddot{\boldsymbol{\xi}}(\mu)\right]\, d\mu + \\ + \boldsymbol{r_B} \times \boldsymbol{R}_{rot}\boldsymbol{F}_B + \sum_{i=1}^{3} \boldsymbol{r}_{Mi} \times \boldsymbol{R}_{rot}\boldsymbol{F}_{Mi} \tag{2.15}$$

Here $\boldsymbol{R}_{rot}$ is the rotation matrix from the global to the local coordinate system. The integral is over the submerged length of the buoy and μ is the distance from the centre of mass.

2.3.1 Harmonic period time

The eigenfrequency or period of a free floating body in heave is only dependent of the hydrodynamic restoring coefficient, c_z, and the mass and added mass of the body.

$$\omega_o = \sqrt{\frac{c_z}{m + m_a}} \tag{2.16}$$

2.4 Irregular wave generation

In order to properly simulate a real loading scenario of the buoy, one cannot use single frequency, sinusoidal waves. The actual sea state is much more complicated and the following subsections will discuss a method to synthesize a possible wave scenario consisting of waves with varying frequency, amplitude, phase and direction, according to Bergdahl (2009). A series of stochastic variables are generated, which determines the specifics for a series of single frequency waves. The principle of superposition is then used to create a seemingly random scenario.

2.4.1 JONSWAP spectrum-amplitude generation

The spectral distribution chosen for the irregular wave generation is the JONSWAP spectrum, which mathematically can be described by:

$$S_J(\omega) = 155\, H_s^2 T_m^{-4} \omega^{-5} e^{-944(T_m\omega)^{-4}} \gamma^{e^{-\frac{(0.191 T_m \omega - 1)^2}{2\sigma}}} \qquad (2.17)$$

With constants chosen as follows for a variable peak period T_m, and H_s being the significant wave height; from Bergdahl (2009).

$$\gamma = 3.3$$

$$\sigma = \begin{cases} 0.07, & \omega \leq \omega_m \\ 0.09, & \omega > \omega_m \end{cases} \qquad (2.18)$$

$$H_s = 1.5\ m$$

$$T_m = 4.6\ s$$

From a uniform distribution of n frequencies around the peak, the spectrum is used to generate suitable amplitudes of the waves so that

$$a_i = \sqrt{2\, S_J(\omega_i)\Delta\omega}\,, \qquad i \in 1,2,\dots,n \qquad (2.19)$$

Here $\Delta\omega$ is the separation between the frequencies, $\Delta\omega = \omega_{i+1} - \omega_i$, and a_i is the chosen amplitude for wave number i.

2.4.2 Phase angle generation

The choice of phase angle, ζ_i for any given wave in the spectrum is more straightforward, as it is taken to be a random number in the region $[0,2\pi]$.

2.4.3 Directionality

The direction of propagation of each wave, θ_i cannot be as random as the phase angle, as the waves normally come from the general direction of the wind. To simulate the directionality of the waves a common distribution of the angles about the x-axis, aptly named the cosine square distribution, is used.

$$D(\theta) = \begin{cases} \frac{2}{\pi}\cos^2(\theta), & |\theta| \leq \frac{\pi}{2} \\ 0, & otherwise \end{cases} \quad (2.20)$$

The uniformly random number $U_i \in [0,1]$ is transformed into the stochastic variable θ_i which will follow the distribution $D(\theta)$ by the use of the inverse transform method.

By setting $U_i \leq \int_{-\frac{\pi}{2}}^{\theta_i} D(\theta)d\theta$ a relation is found between the two values as

$$U_i \leq \frac{1}{2\pi}(2\theta_i + \pi + \sin(2\theta_i)), \quad (2.21)$$

And θ_i can be found as the smallest value of θ_i that satisfies (2.21).

2.4.4 Example spectrum

By combining the stochastic variables for each component and superposition of the resulting wave components, the following expression is finally obtained.

$$\Phi = -\sum_i \frac{a_i\, g}{\omega_i} \frac{\cosh\big(k_i(H+z)\big)}{\cosh(k_i H)} \cos[k_i \kappa_i - \omega_i t + \zeta_i] \quad (2.22)$$

$$\kappa_i = -x\cos(\theta_i) - y sin(\theta_i)$$

Here follows an example of an irregular wave, and its different components.

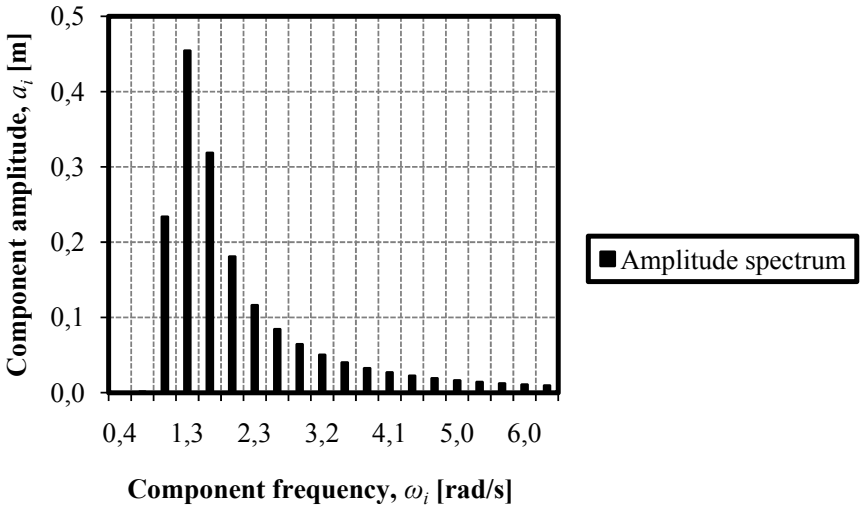

Figure 2.2 A typical JONSWAP spectra obtained from making amplitude choices according to (2.19). The frequencies are evenly distributed.

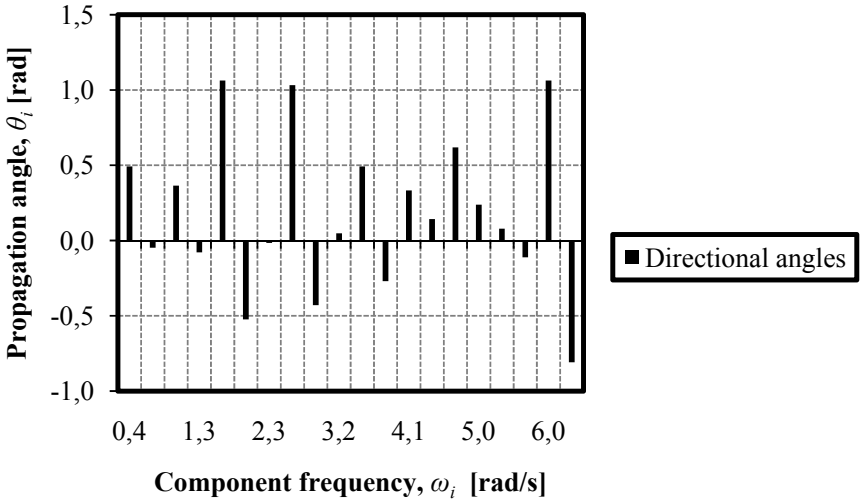

Figure 2.3: A typical result for the cosine square distribution. Note how most of the points are centered around $\theta_i = 0$.

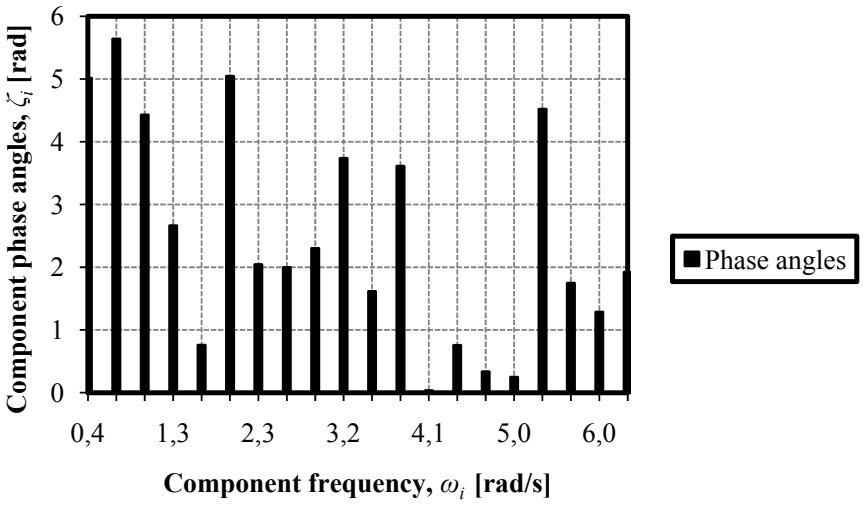

Figure 2.4: The random distribution of phase angles in the region $\zeta_i \in [0,2\pi]$.

The contribution from these components are added using (2.22) to produce the following, seemingly random, wave form appearance.

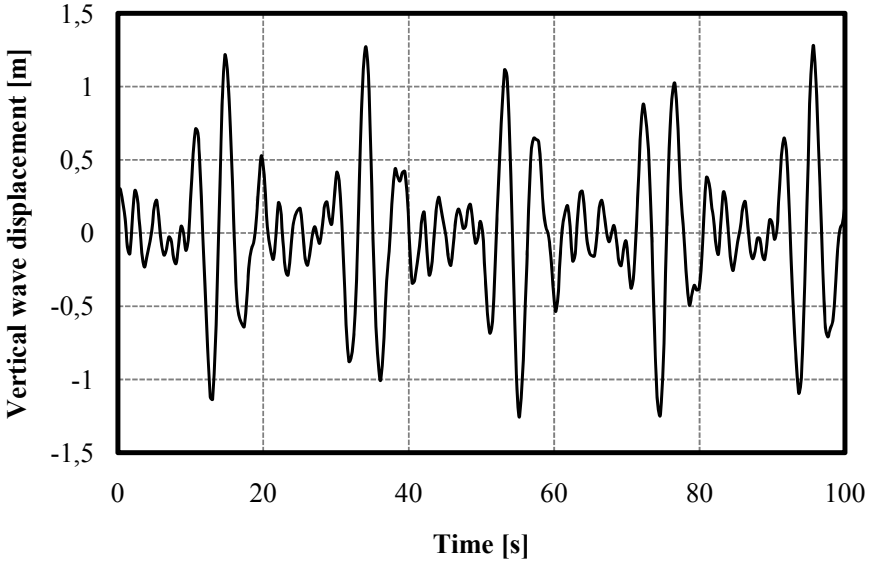

Figure 2.5: The resulting random synthetic wave form during an example simulation time length of 100 *s at the position of the buoy,* $[x, y] = [0,0]$. *The repetition time is* $T_R = 20$ *s.*

2.5 Time integration schemes

The dynamic analysis has been performed using Newmark's time integration method. Let for now U_t denote the displacement of any degree of freedom in the system at time t, and its corresponding values of the velocity and acceleration be denoted by $\dot{U}_t$

and $\ddot{U}_t$. The method is actually a collection of methods where the setting of $[\alpha, \delta]$ defines the type of analysis.

$$\dot{U}_{t+\Delta t} = \dot{U}_t + \left[(1-\delta)\ddot{U}_t + \delta\ddot{U}_{t+\Delta t}\right]\Delta t \qquad (2.23)$$

$$U_{t+\Delta t} = U_t + \dot{U}_t\Delta t + \left[\left(\frac{1}{2} - \alpha\right)\ddot{U}_t + \alpha\ddot{U}_{t+\Delta t}\right]\Delta t^2 \qquad (2.24)$$

Two types of analyses are performed in this thesis. One explicit, $[\alpha, \delta] = [0,0]$, which is the common Euler forward method, and one implicit where $[\alpha, \delta] = \left[\frac{1}{4}, \frac{1}{2}\right]$. The latter is the unconditionally stable algorithm of constant average acceleration.

The explicit analysis is computationally cheap at each time step, due to its simplicity, but it has a stability criterion which puts an upper limit on the time step. In order for explicit algorithms to work in a FE setting the time step size cannot be larger than the time taken for a longitudinal wave to travel a distance equal to the smallest element size, dL_{min}. In mathematical terms Δt must fulfill the following relation in order to ensure stability in the time integration.

$\Delta t < \frac{dL_{min}}{\sqrt{K/\gamma_0}}$, from Lindahl/Sjöberg (1983) *(2.25)*

Here K is the tangential stiffness and $\gamma_0$is the mass per unit length of the mooring line. In this case, the criterion of stability is very difficult to meet, and as the force response of a strain in the line is of non-linear type, K varies in time and it is therefore difficult to choose Δt. In order to get a good result, one would ideally want $dL_{min} \rightarrow 0$. This will of course never be the case, but it points to that a high-resolution analysis with many elements will lead to that Δt becomes so small that another solution technique is needed to simulate longer time spans with reasonable speed.

As a consequence of this, an implicit method has been developed, and is the one used in the simulation of the results in Section 4. The model looses some of the accuracy in the time integration as very fast transients are smoothed over the larger time step and some phenomena might be lost in that process. The implicit algorithm ensures stability, but the amount of operations per time step increases as the non-linear form of the problem makes a direct time integration impossible. Instead one must make use of an iterative process.

2.6 Non-linear solution strategy – BFGS method

When dealing with non-linear problems in a finite element setting, there are a number of different methods available. Newtonian algorithms are the most common and they

are all based on the same algorithm, beginning with the setting up of the error function. In this case the error function represents the force imbalance at each node.

$$\boldsymbol{g} = \boldsymbol{M}\ddot{\boldsymbol{r}} + \boldsymbol{K}\boldsymbol{r} - \boldsymbol{F} \tag{2.26}$$

Here $\boldsymbol{M}$ and $\boldsymbol{K}$ are the mass- and stiffness matrices of the system and $\boldsymbol{r}$ is the position vector of all free degrees of freedom.

The time integration scheme gives a relation between $\ddot{\boldsymbol{r}}$ and $\boldsymbol{r}$, and in this non-linear setting the matrices $\boldsymbol{M}$ and $\boldsymbol{K}$ and the load vector $\boldsymbol{F}$ are all dependent on the state vector $\boldsymbol{r}$. Let $\boldsymbol{r_0}$ be the correct solution, so that $\mathbf{g}(\boldsymbol{r_0}) = \mathbf{0}$. Now find the derivative of the function, i.e. the Jacobian matrix $\boldsymbol{J}$, at a given guess $\boldsymbol{r}^*$. Here n is the number of free degrees of freedom.

$$\boldsymbol{J} = \frac{\partial \boldsymbol{g}(\boldsymbol{r}^*)}{\partial r_i^*} \ , \ \ i \in 1,2,\dots,n \tag{2.27}$$

In search of $\boldsymbol{r_0}$ we need a $\boldsymbol{dr}$ so that $\boldsymbol{dr} + \boldsymbol{r}^* = \boldsymbol{r}_0$. This new step direction is defined by $\boldsymbol{J} = \frac{\boldsymbol{g}(\boldsymbol{r}^*) - \boldsymbol{g}(\boldsymbol{r}_0)}{\boldsymbol{dr}}$, or more explicitly in equation (2.28).

$$\begin{aligned} \boldsymbol{dr} &= -\boldsymbol{J}^{-1}\boldsymbol{g}(\boldsymbol{r}^*) \\ \boldsymbol{r}_{k+1}^* &= \boldsymbol{r}_k^* + \boldsymbol{dr} \end{aligned} \tag{2.28}$$

Here k is the iteration number.

Thus $\boldsymbol{dr}$ is the step that minimizes the error function, given that the Jacobian matrix remains constant between $\boldsymbol{r}^*$ and $\boldsymbol{r}_0$. This however is seldom the case, especially not in the case of strong non-linearities, and therefore it is necessary to repeat this process iteratively to find the correct solution. In order to do so the Jacobian needs to be updated. This is where the different methods differ. In the classical Newton-Raphson method, the Jacobian would be calculated again using (2.27), but as this requires a number of n^2 operations, and then an inversion of the resulting n by n matrix, this is a costly approach. The BFGS method has been used instead in this thesis, with the addition of the Sherman Morrison formula. The first is an update where the old Jacobian is used as a base, and two symmetrical matrices computed from the change in position vector, $\boldsymbol{dr}$, and in the error function, $\boldsymbol{dg}$, are added as perturbations. The Sherman Morrison formula is a way of updating the inverse of the matrix directly and (2.29) shows the final update of the inverse of the Jacobian. Here k is the iteration number.

$$\boldsymbol{J}_{k+1}^{-1} = \boldsymbol{A}_k^{-1} - \boldsymbol{B}_k^{-1}$$

$$\boldsymbol{A}_k^{-1} = \frac{(\boldsymbol{dr}^T\boldsymbol{dg} + \boldsymbol{dg}^T\boldsymbol{J}_k^{-1}\boldsymbol{dg})\boldsymbol{dr}\boldsymbol{dr}^T}{(\boldsymbol{dr}^T\boldsymbol{dg})^2} \qquad (2.29)$$

$$\boldsymbol{B}_k^{-1} = \frac{(\boldsymbol{J}_k^{-1}\boldsymbol{dg}\boldsymbol{dr}^T + \boldsymbol{dr}\boldsymbol{dg}^T\boldsymbol{J}_k^{-1})}{(\boldsymbol{dr}^T\boldsymbol{dg})}$$

2.6.1 Line search

Line search, or damped Newton, algorithms are used to optimize the step size $\boldsymbol{dr}$. The step is not just $\boldsymbol{dr}$ but is instead taken to be $\alpha\boldsymbol{dr}, \alpha \in [0,1]$. In this way, the line along the direction of $\boldsymbol{dr}$ is searched for the step length that will produce the lowest value of the norm of the error function, $\|\boldsymbol{g}\|$. The program has the ability to use the line search algorithm; however it was seldom needed to increase the convergence rate.

3 Method

3.1 Geometry and coordinate systems

It is convenient to start with some definitions that will be used later on in this chapter. First of all; Figure 3.1 below shows the initial configuration of the system, seen from the side.

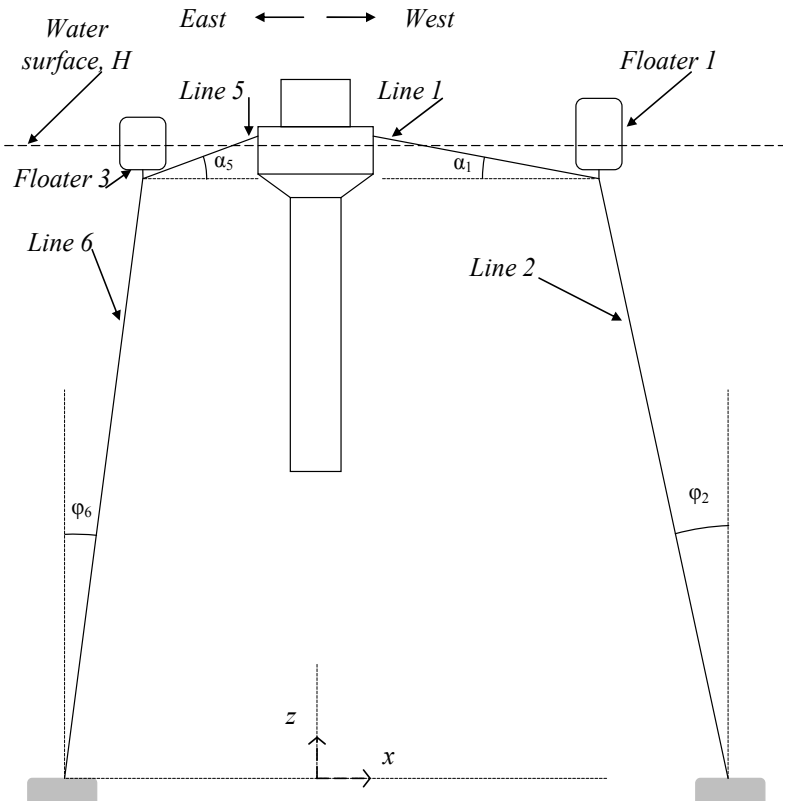

Figure 3.1: Schematic drawing of line system in x-z plane. The picture is not according to scale.

The buoy is moored using a total number of six mooring lines. Three of these are fastened to the buoy, and are connected to floaters 15m away. These floaters are each in turn connected to concrete anchors at the seabed with an additional line of unstretched length 40m, which is the same as the water depth on site. Figure 3.2 shows the initial line configuration as seen from above.

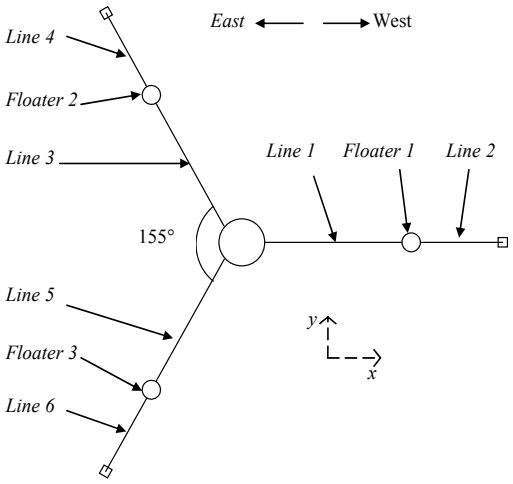

Figure 3.2: The initial line configuration seen from above. Note that this image is not according to scale.

The origin of the global coordinate system has been placed exactly beneath the centre of mass of the generator buoy, on the seabed, as it would be in calm sea. The origin compensates for the stationary effect of water current and all positions in the simulations are given with respect to this point. The origin is fixed and remains so as the buoy is allowed to respond to wave and mooring forces and may drift away from its equilibrium position. The corresponding axes are oriented such that $\hat{x}$ points straight to the west, and $\hat{z}$ points vertically upwards. There is another coordinate system which is body-fixed to the buoy with origin in its centre of mass. All moments acting on the buoy are calculated around this point, and the movement of it is described by the position, velocity and acceleration of the centre of mass, as well as angular displacement, velocity and acceleration about the global system axes.

3.1.1 Motion description

When dealing with the dynamics of ships and other mobile structures in water, it is common to use a separate notation for the motion of the body. The motion of the buoy in the three global coordinate directions, x, y and z is referred to as the surge, sway and heave motion respectively. In a similar way, the angular displacement of the buoy about the x- ,y- and z-axes are described by the terms roll, pitch and yaw.

3.2 Stimuli of the system

The exciting external force from the waves has been simulated in two separate ways; using a prescribed displacement of the buoy, and allowing it to respond to the motion of the waves.

3.2.1 Prescribed displacement

The simplest approach is when the system is given stimulus by a prescribed motion of the generator buoy. This has no real application when it comes to an analysis of the buoy response to wave loading, but it is a helpful tool when the model is to be validated against the measurement data from the buoy site outside of Vinga. As the exact wave conditions might be difficult to ascertain, this type of simulation can be used to approximate the influence of the waves on the moorings, given that the buoy moves in the same way as in reality, but in a simulated environment of calm water.

This approach has two major setbacks, besides its inaccuracy. It cannot account for resonance effects, nor can it take into account a phase lag between the movements of the device and the floater due to wave loading. In the deformation controlled simulation, all movement of the floaters is a consequence of the buoy displacement. When the waves are allowed to act on the entire system, the independent movement of the floaters can also be taken into account.

3.2.2 Wave induced response

The wave induced response is derived from the linear wave theory described in Section 2.2. Initially the system is at equilibrium and at rest, and the wave loading starts at $t = 0$. To avoid the numerical impulse this might have on the system, the amplitude of the wave is ramped up to its proper value during the first $30\,s$ of simulation. In this way, the effect of the remaining transients after ramping is also decreased, compared to the value after a sudden impact of the plane wave. As the mooring system and geometry of the buoy is symmetric with respect to mirroring about the x-axis, only waves from the first and second quadrant of the *xy*-plane are taken into account. 9 different directions of propagation are considered in the simulations.

$$\theta_w = \frac{n\pi}{8}\,, \qquad n \in 0,1,2,\ldots,8 \tag{3.1}$$

Here $\theta_w = 0$ corresponds to a wave coming directly from the west, and $\theta_w = \pi$ correspond to a wave coming from the east. See Figure 3.3 for clarity.

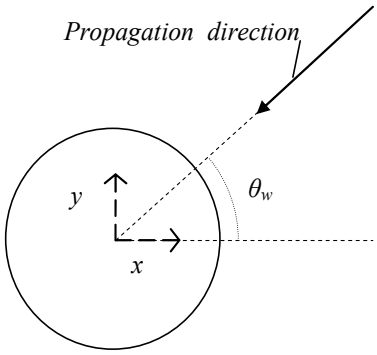

Figure 3.3: The definition of θ_w as a description of the direction of propagation of the wave.

The waves used in the systematic simulations are all regular waves with a single frequency. The response will be quite different for naturally occurring irregular waves composed of many different frequencies and wave heights. The regular waves have been used as a way of isolating different parameters to study their effect on the response individually.

3.2.3 Simulation of the water current

Two major assumptions are made about the water current at the site of the buoy. Throughout the simulations, no vertical component of the current has been tried, so all current velocity is assumed to be in the *xy*-plane. Furthermore, the water current is assumed to be linearly dependent on the depth, to have its maximum value at the surface, and to be one third of that value at the seabed.

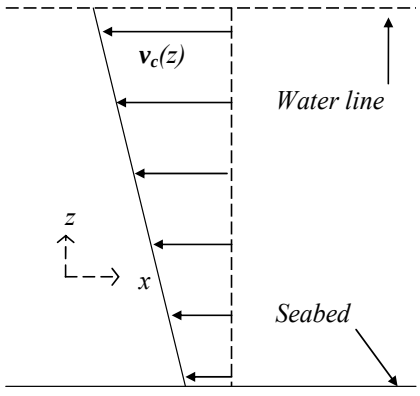

Figure 3.4: Showing the assumption made about the vertical decline of the water current magnitude.

The MATLAB program is written to take any direction of water current, however the simulations have been restricted to the same angles, θ_c, as was used in the wave simulation, see (3.1) and Figure 3.3.

3.3 Parameter approximation

As discussed in chapter 2 the governing equations are dependent on different parameters.

3.3.1 Drag coefficient

The choice of drag coefficient is rather complicated and very difficult to validate. A combination of two theories has been chosen for use in this thesis. First of all Figure 3.5 show the dependence on absolute maximum speed of the water, in the form of Reynolds number.

$$Re = \frac{v_{max} d}{\nu} \qquad (3.2)$$

Here ν is the kinematic viscosity of the water, d is the diameter of the body, and v_{max} is the maximum speed of the water obtained from the vector sum of the current- and wave velocity.

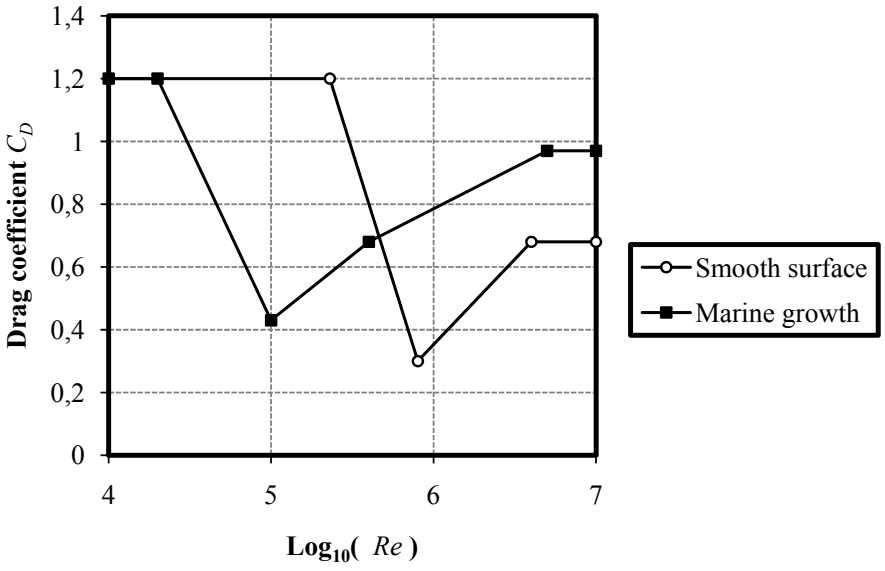

Figure 3.5. The approximated drag coefficient as a function of the Reynolds number, Re, of the wave and sea current loading scenario. Figure from D.N.V (2000)

There is a clear difference between the two lines in Figure 3.5, as the surface roughness clearly has an impact on the drag force. Furthermore the drop in C_D, seen at $Re = 10^5$ and $Re = 8 * 10^5$ respectively represents a change in the boundary layer surrounding the structure which creates more turbulent flow where the flow theory becomes more complex. This drop naturally comes at a lower maximum velocity for

the growth-covered surface than for the smooth one, as the growth creates a disturbance in the fluid.

The values obtained from Figure 3.5 are valid for two-dimensional circular sections, or in three dimensions: infinitely long cylinders. The values are therefore multiplied by a correction factor ϵ depending on the ration between the length and diameter of the cylinder in question. Table 3.1 shows the correction factors for the three types of bodies used in this thesis.

Table 3.1: The length-diameter ratio of the different bodies and the corresponding correction factor for the drag coefficient, C_D.From Mårtensson (1988)

Body	Length-Diameter ratio, $\frac{L}{d}$	Correction factor, ϵ
Buoy	10	0.8
Float 1	2	0.6
Float 2 & 3	1,36	0.6
Lines	416	1

3.3.2 Added mass approximation

The added mass is in reality a frequency dependent variable which also is affected by other factors. D.N.V (2000) for instance, covers the effect of a barrier in the vicinity of the body and Mårtenson (1988) covers the complete diffraction that leads up to the frequency dependence. However the conclusions are drawn for spheroids and ellipsoids on or near the surface and the bulk of the added mass for the buoy is totally submerged. This is why the constant added mass of the 2D sections representing a circular plate and the infinitely long cylinder, has been used in this thesis. The numerical values of these quantities have already been presented in section 2.1.1.

3.3.3 Radiation damping coefficient

The parameter for radiation damping is naturally extremely dependent on the geometry of the body. The special case of the buoy is in this setting seen as equivalent to a sphere that is semi-submerged. The ratio between radius and draft of this hypothetical sphere is taken to be 1. The radiation damping coefficient is also highly dependent on the frequency of oscillation. Based on figures from Mårtenson (1988) the following approximation of the frequency dependence of $b_x = b_y$ for surge and sway, and b_z for heave, has been produced and used in the simulations.

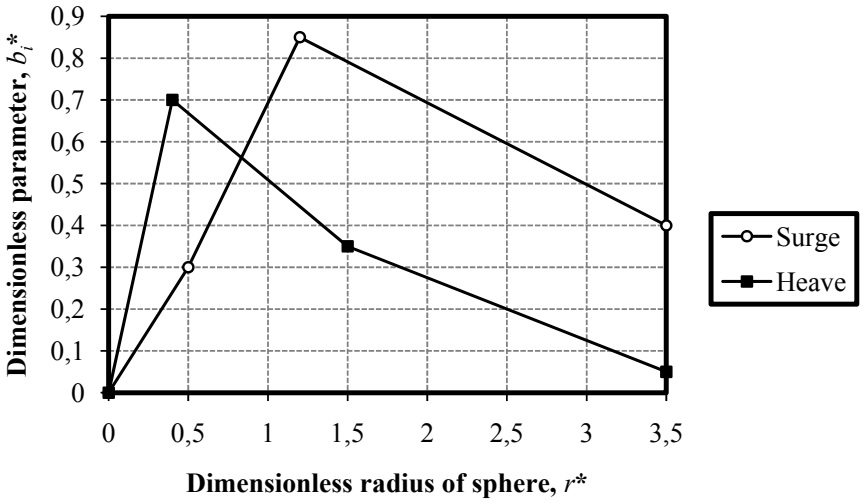

Figure 3.6: The radiation damping coefficient of surge/sway and heave motion as a function of radius and frequency of the waves. Figure from Mårtensson (1988)

Here $r^* = r\omega^2/g$ and $b_i^* = \frac{b_i}{\rho_w \omega\, r^3}$. The effect of damping due to the roll and pitch motion, and the coupling effects between the forces from radiation damping in the different directions are not considered in the simulations.

3.4 Equations of motion - simulation in practice

There are three different types of bodies in the system, each with their own mathematical modelling approach. The generator buoy is treated as a rigid body with six degrees of freedom, the line element as a two node element in a finite element setting, and the floaters affect some connection nodes with point forces and masses.

3.4.1 Simulation of the buoy

The buoy itself is a very complex structure, and one could write a master's thesis on the simulation of flow in and around the buoy alone. The effects of these small scale details are however negligible in their contribution to the mooring forces. Therefore a simple geometrical model of the generator buoy has been put together and here follows a short description of the assumptions made.

All parts of the buoy are assumed to be completely cylindrical. The following approximations strongly affect the resulting centre of mass, $\boldsymbol{r}_c$, and the moments of inertia, $\boldsymbol{I}_c$ of the buoy. The buoy is divided into 7 parts, each with an assigned mass, and they are all taken to be hollow cylinders, with varying inner and outer radii. Parts I-IV in Figure 3.7 contains most of the dry mass of the buoy, whilst the walls of the plastic pipe, Part VI, fill with water and become much heavier when submerged.

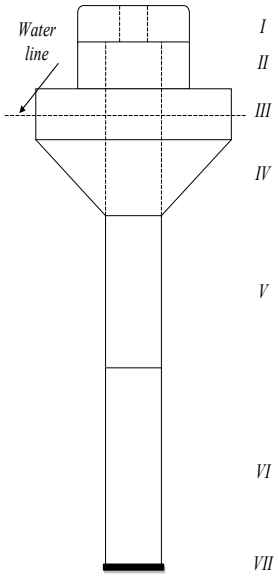

Figure 3.7: The geometrical description of the buoy used in the simulations. The mass and inertia of the different parts have been calculated separately and added to a single centre of mass for the buoy. Figure is not according to scale.

The buoy element is given special care in this thesis as it is by far the most dominating structure in the system. The scale of it makes even the slightest displacement result in huge forces. It is seen as a rigid body and it is assumed to be at a static equilibrium when the mooring line attachments are situated 0.5 m above the mean water level. This makes the static forces from gravity and buoyancy cancel and the resulting equation of motion can be expressed as a system of equations composed of (2.13), (2.14) and (2.15).

These equations form a system of six equations, one for each degree of freedom, which is solved for each time step in the simulations. The mass matrix of the buoy must be assembled each time as it changes with the angular displacement. The added mass is constant in the local buoy coordinate system but varies in relation to the global and must be transformed by the use of a rotation matrix. The mooring forces and moments come from the tension forces in the lines, which are calculated in an earlier stage of the iterations process. The drag force is approximated by a numerical integration over the length of the bottom pipe. This is done because of the strong gradient of the water velocity in the vertical direction. The water particle velocity is thus evaluated at each depth and the corresponding relative velocity and drag force contribution are computed.

The mass, added mass and the hydrodynamic restoring coefficient c_z are all dependent on the configuration of the piston. Therefore two configuration cases have been considered in this thesis, corresponding to the locking or unlocking of the piston of the generator. It is simulated to be completely free, and thus vertically unconnected to the generator, or locked and bound to the position of the buoy. The main difference between the two is that the centre of mass is lower in the locked configuration as the water column inside the plastic pipe is included in the mass of the buoy. The positions of the centre of mass are given in Table 3.2 below. The reason for the low position of

the centre of mass is that the outer shell of the lower plastic pipe is hollow and is filled with water of a total mass of $3902kg$.

Table 3.2: Table describing the position of the centre of mass of the buoy and its change due to the locking or unlocking of the piston.

Piston configuration	Distance from bottom of buoy to centre of mass
Free / Unlocked	13.7 m
Locked	11.3 m

Another major difference between the computation of the forces on the buoy for the locked and free piston position is the computation of the pressure force at the bottom. The contribution from the sloping part of the bottom is identical between the two simulations, but when the buoy is locked the contribution from the bottom of the lower pipe, part VII in Figure 3.7, must be added.

3.4.2 Simulation of line elements

3.4.2.1 Material data and assumptions

The mooring line itself is simulated using a numerical approximation of its load response curve obtained from the www.bridon.com. Figure 3.8 shows the approximation that is used as the $F - \epsilon$ relation of the line. The two separate graphs in Figure 3.8 represent the response of the line in a new and worked condition respectively. In practice the line will probably not, at any given time, follow any of these graphs exactly; but will always follow a path that lies in between them. In this sense they represent the extreme cases of very new and very old line, and, as the rate of degeneration of the line is unknown, the modelling has been restricted to these two cases of line status.

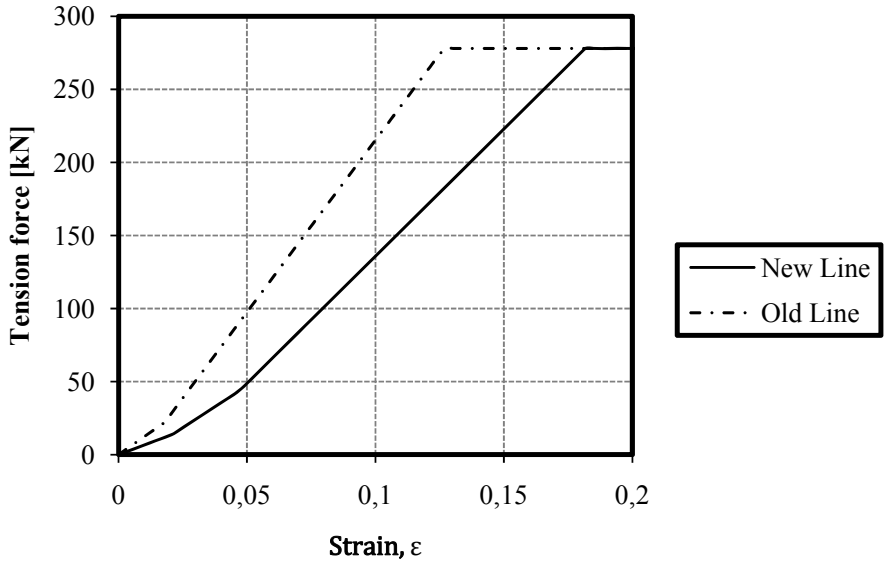

Figure 3.8: The responsive force in the mooring line to an elongation. The breaking force is 278kN

Two major assumptions are made in the simulation of the mooring line. First of all the lines will be simulated without any internal viscosity. Physically this means that the lines will function as ideal springs with no internal damping, and mathematically the tension force in the line is modelled as $F = K\epsilon - C\dot{\epsilon}$, where $C = 0$. Secondly they are assumed to be unaffected by the twist around the symmetry axis. If a line is twisted instead of straight it will have the effect of increased stiffness in axial loading. In this system, however, there is nothing that can sustain any large twist loading, and the total error due to this phenomenon should be relatively small.

3.4.2.2 Equation of motion

The mechanics of the mooring lines is very much dependent on the direction of the motion. The following equation has been implemented in a FEM setting and integrated over each element to produce the nodal displacements.

$$\gamma\ddot{\mathbf{r}} + \gamma_a(\ddot{\mathbf{r}} - \hat{\boldsymbol{t}}^T\ddot{\mathbf{r}}\,\hat{\boldsymbol{t}}) = -\gamma_e g\hat{\boldsymbol{z}} + \boldsymbol{F}_{drag} + (\rho_w A + \gamma_a)\ddot{\boldsymbol{\xi}} + K\epsilon\hat{\boldsymbol{t}} \qquad (3.3)$$

Here γ is the mass per unit length of the cable. $\gamma_e$and γ_a are the effective and added masses per unit length of the submerged cable, and A is the area of the cross-section. As the lines are so slender and only the line edge elements are affected by it, the added mass in the tangential direction is neglected in (3.3). The effective mass per unit length is defined by equation (3.4) below.

$$\gamma_e = A\frac{\rho_{line} - \rho_w}{\rho_{line}} \qquad (3.4)$$

Thus, $\gamma_e g\hat{\mathbf{z}}$ in (3.3) represents the combined effect of the gravitational and the buoyancy force on the submerged line. As the level of submersion of the three horizontal lines varies, some compensation for this must be incorporated into equation (3.3). This is solved by simply changing the values of γ_a and γ_e, by a function of the fraction of the line which is currently submerged. In mathematical terms; if an element is partly submerged with a fraction, $\beta \in [0,1]$, of its length below the water surface then $\gamma_a$and $\gamma_e$in (3.3) are replaced by γ_a^* and γ_e^* respectively.

$$\begin{aligned} \gamma_a^* &= \beta\gamma_a \\ \gamma_e^* &= \beta\gamma_e + (1-\beta)\gamma \end{aligned} \qquad (3.5)$$

This method yields a good approximation of the total force on the element, but it is less accurate in determining the force distribution across the element length as the resulting force of buoyancy and gravity affects the two nodes of the element by an equal amount. As the lines are so light, especially in comparison with the magnitude of their elastic internal forces, the error from this approximation will not be that large.

3.4.2.3 Finite element approximation

Each line is divided into a number of elements of un-stretched length dL. Each element consists of two nodes of three degrees of freedom; so the position of node n can be described by $\boldsymbol{r}_n = \begin{bmatrix} x_n \\ y_n \\ z_n \end{bmatrix}$. In accordance with Lindahl/Sjöberg (1983), no rotational modes are taken into account as the line is supposed to have no internal bending stiffness. Furthermore, each element is supposed to keep the straight appearance, so that one line is in effect simulated by a system of joints that sustain no moment, and bars that cannot bend. The only internal force in the line is the tension force which is directed along the axis of the line element. Thus a system of elements of six degrees of freedom each is setup using linear approximations of the shape functions. Each element is analysed using a parameterization of the tangent direction so that the shape functions are one-dimensional and can be expressed by the dimensionless parameter α.

$$\begin{cases} \phi_1 = 1-\alpha \\ \phi_2 = \alpha \end{cases} \quad \alpha \in [0\,,1] \qquad (3.6)$$

All positions, velocities, accelerations and forces are thus assumed to vary linearly along each line element.

Furthermore the lumped mass technique has been used, which means that the distributed mass of the mooring line element is lumped into the two nodes at its ends. Mathematically this is described by using constant shape functions for the mass matrix integration so that (3.6) instead is transformed to (3.7).

$$\begin{cases} \phi_1 = 1 \;\; \phi_2 = 0 & \alpha \in [0, \frac{1}{2}] \\ \phi_1 = 0 \;\; \phi_2 = 1 & \alpha \in [\frac{1}{2}, 1] \end{cases} \tag{3.7}$$

3.4.3 Floater simulation

The floaters are simulated as rigid bodies with only three degrees of freedom. The motion is described by the midpoint of the lower end, at the connection point with the lines. As the motion is restricted to the translational degrees of freedom, the floaters are assumed to be vertical cylinders at all times. This is of course not the case, but in a submerged position it is fairly accurate as the vertical buoyancy force is the dominating term in the moment equation. There are two types of floaters where one is between line number one and two of the mooring leg one with a maximum buoyancy force of $18\ kN$ in totally submerged position. The mooring legs two and three have identical, somewhat smaller floaters with a corresponding buoyancy force of $11\ kN$.

The dynamic analysis is carried out in a quasi-static setting. At each time step, the level of submersion is computed and the corresponding buoyancy force calculated. The added mass, wave, drag and gravitational forces are all computed and the resulting effective masses and external forces are added as point masses and forces to the connection node equations. The following equations of motion have been used, where there is no moment equation as the floaters only are allowed three degrees of freedom.

Heave: $$(m_z + m_{az})\ddot{\eta}_z = m_{az}\ddot{\xi}_z + + c_z(\xi_z - \eta_z) + F_{Mz} + F_{Dz} \tag{3.8}$$

Surge: $$(m_x + m_{ax})\ddot{\eta}_x = (\rho_w V + m_{ax})\ddot{\xi}_x + F_{Mx} + F_{Dx} \tag{3.9}$$

3.5 Numerical Analysis

3.5.1 Non-linear iteration process

To solve the problem using an implicit time algorithm the non-linear iteration method BFGS, with the addition of the Sherman-Morrison formula and a line search algorithm, has been used. A schematic walkthrough of the iteration process and a theoretical description of the mathematical tools are presented in section 2.6. Using this method, a step direction is computed and a new trial state vector is produced. The model checks that this is a better guess than the previous one and then proceeds. If this should not be the case the Jacobian of the previous guess is instead calculated explicitly using the Newton-Raphson method, which is costly but accurate in its resulting Jacobian approximation. In this way it is ensured that if the first guess at

each new time step (which is produced using the explicit time integration scheme of section 2.5) should be very far from the true value, and the BFGS approach should not work; the convergence is ensured by the intervention of the Newton method.

3.6 Initial conditions – Static equilibrium

The initial configuration of the model is calculated for a certain set of prerequisites which normally does not occur. First of all the system is assumed to be in calm water with no current. Secondly the "horizontal" lines to the generator buoy are assumed to be exactly 0.5 m above the water surface. The system is defined by the preset variables of line lengths and buoy and floater dimensions; with the additional prerequisite in the strain in line two, see Figure 3.2. This prescribed strain is needed to define the exact configuration of equilibrium of the line system. There is no external load on the system during the first time step so the initial acceleration and velocity are both approximately zero for all degrees of freedom. In the case of a sea current, it is applied to this state of the system and a new, updated equilibrium state is obtained. The origin is moved to the new buoy point in the xy-plane and the simulation in time can begin.

The advantage of starting the simulations from an equilibrium point is that all movement in the system comes from the stimulus it is subjected to, and so the analysis of the results is more simplified then had otherwise been the case.

4 Results

4.1 Default settings

In order to maintain comparability between different simulations, a standard default set of system and load parameters have been defined. This was found to be useful as the effects of different parameters and load scenarios have been investigated independently. If nothing else is specified, the results are from the set of program parameters and load scenario presented in (4.1).

- $T = 4$ s
- $a = 0.5$ m
- $\theta_w = 0$ rad
- $|\boldsymbol{v}_c| = 0$ m/s
- $\theta_c = 0$ rad
- $\epsilon_2 = 0.01$
- $T_{end} = 100$ s
- Two elements per horizontal mooring line.
- One element per vertical mooring line.
- Piston is free and vertically unconnected to the generator.
- No marine growth on any parts of the system.
- New mooring lines.

(4.1)

The total simulation time, T_{end}, has been judged to be sufficient to encompass both the transient responses as the wave train hits the structure, and the stable oscillation, when these transient effects have died down. The load parameter combination of period time, T, wave amplitude, a, and wave train angle of attack, θ_w, are defining the incoming wave. When these have the values of (4.1) it is defined as the standard or default wave. As an example of the use of these default settings the investigation of the effect of wave period for instance, is done by keeping all parameters in (4.1) fixed, and only vary the wave period time, in order to properly isolate its effect.

4.2 Number of elements per line

Finite element modelling and computation is always a balance between computational speed and a high accuracy in the results. The addition of more elements increases the number of computations per time step and also puts numerical demands on the convergence so that the time step size must be decreased, which of course slows the program down significantly. The following two figures show the result of a resolution investigation where the tension forces in the lines are the mean values of the different element tensions. This is of course an approximation in itself as the actual tension response for lines with more than one element includes more modes of higher frequencies, which are not seen here. These varying tensions are of a smaller scale and are of decreasing individual amplitudes, but increasing in numbers as the element size goes to zero as an effect of the principle of lumped mass being more accurate and

that higher modes are encompassed by the simulation. It has not been possible to investigate this further within the scope of this thesis, and the results are therefore focused on the first mode of the tension response in the different mooring lines.

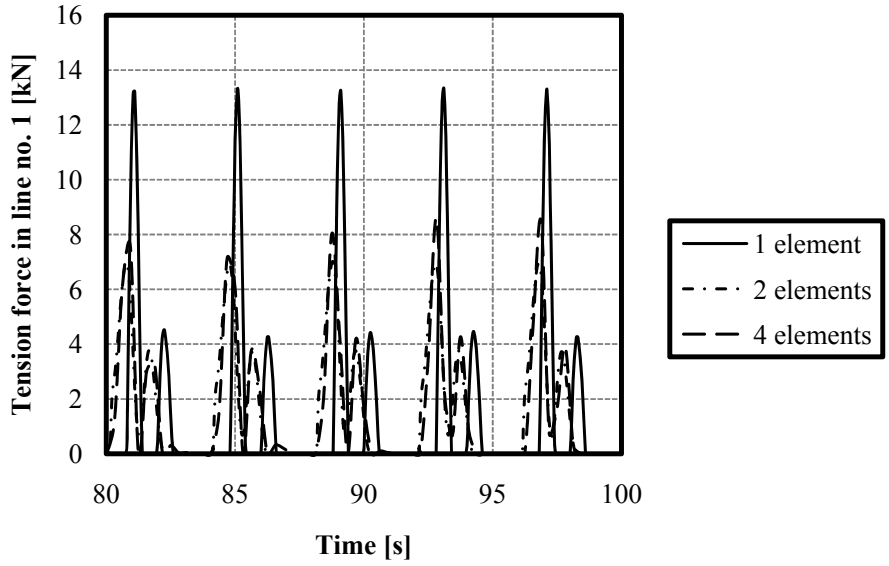

Figure 4.1: The time response of the default wave in line number one between 80 *and* 100 *s of simulation. A comparison between different number of elements on the line.*

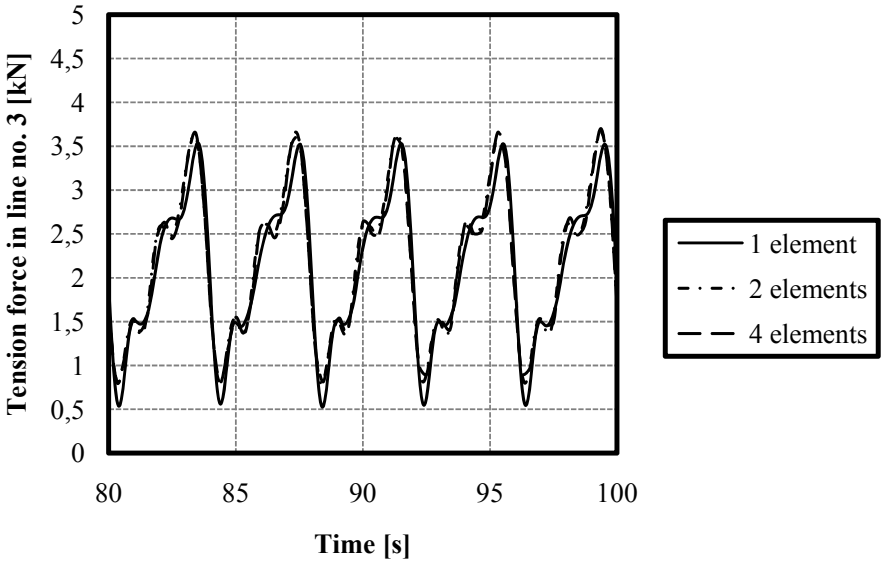

Figure 4.2: The time response of the default wave in line number three between 80 *and* 100 *s of simulation. A comparison between different number of elements on the line.*

As can be seen from Figure 4.1, the simple resolution of one element per line cannot be used with satisfactory result. It is clear however that the difference between one and two elements per line is much greater than that between two and four elements, from which the conclusion is drawn that two elements per line gives a satisfactory

approximation of the tension force response in the horizontal mooring lines. Figure 4.2 shows that the simplest resolution is a good approximation for the tension in lines that does not go slack and the simulation of the vertical mooring lines is therefore conducted with one element per line.

4.3 Eigenfrequencies and impulse load response

To study the eigenfrequencies of the system the buoy was subjected to an impulse load of $50\,kN$ during one timestep of $\Delta t = 0.05$ s, in the direction of the three coordinate axes $\hat{x}, \hat{y}$ and $\hat{z}$ individually. As the vertical motion of the buoy affects the horizontal motion of the floaters, these experiments are of course coupled and the same frequencies are seen to various extents in the different tests. The resulting time response has been analysed using Fourier transformation and the resulting transformed signal has been normalised by its maximum value.

4.3.1 Heave impulse loading

4.3.1.1 Theoretical prediction

The eigenperiod of the buoy in heave is dependent on the piston configuration as this alters both the hydrodynamic restoring coefficient and the mass and added mass of the buoy, see (2.16).

Table 4.1 shows the values of the affected parameters and their eigenperiod according to (2.16), for the two configurations of the piston position.

Table 4.1: The difference between the locked and free configuration of the piston when it comes to the hydrodynamic restoring coefficient, mass and added mass of the buoy. Also seen is the theoretical harmonic period for the two cases for a buoy in heave without moorings.

Piston conf.	c_z [kN/m]	m_z [tonnes]	m_{az} [tonnes]	T_0 [s]
Free	108	13.69	12.92	3.118821
Locked	126	49.99	14.41	4.491977

4.3.1.2 Simulation results

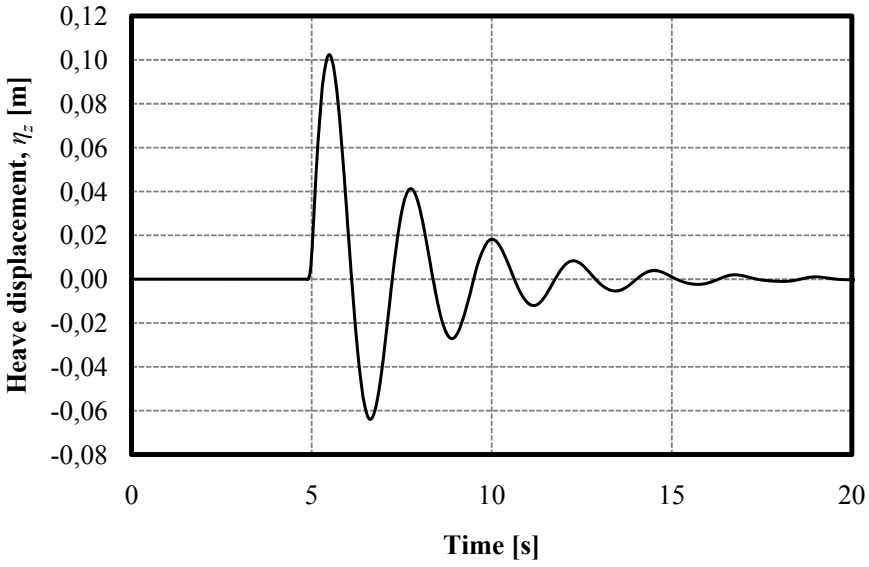

Figure 4.3: The heave response to a vertical impulse load of 50kN. The piston position is free in this simulation.

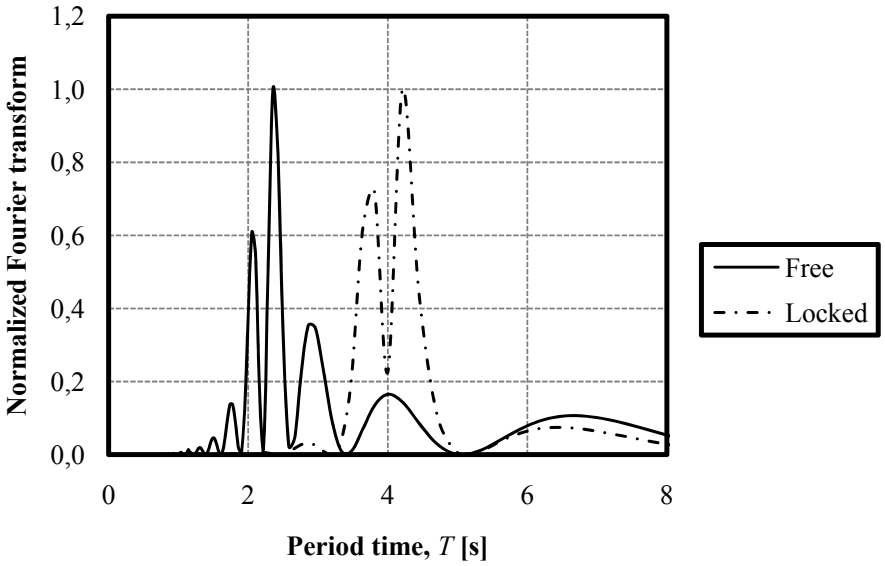

Figure 4.4: The Fourier transformation of the heave motion response to a 50kN impulse load directed in the positive vertical direction $\hat{\mathbf{z}}$. The figure shows a comparison between the eigenperiods of the buoy in heave motion when the piston position is locked and free respectively.

Figure 4.4 shows the Fourier transform of the heave motion response on the impulse load. There is a distinct shift in eigenperiod between the two configurations of the

piston from $T_H = 2.35\,s$ for the free piston to $T_H = 4.21\,s$ for the locked configuration. As the generator is activated and a varying amount of work is taken out of the system, the harmonic period, T_H, will vary but will remain in between the two values from Figure 4.4.

The harmonic periods are somewhat shorter than predicted in Table 4.1. In the case of for instance a ship, without any moorings, the actual harmonic period is normally slightly longer than is predicted by (2.16), due to the effect of radiation damping. In this case the buoy is fastened by three elastic, taut mooring legs and it is therefore a reasonable assumption that this tension serves to decrease the period time of the harmonic oscillation.

By looking at the Fourier transform of the tension response in the horizontal mooring lines the eigenperiods of the mooring legs can also be approximated from this type of analysis.

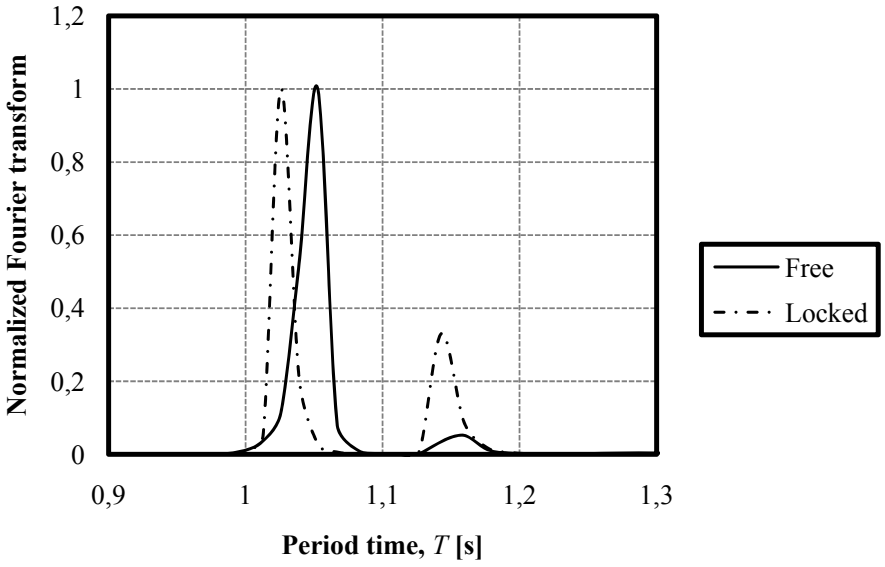

Figure 4.5: The Fourier transform of the tension force response in line number one. The load was in this simulation a vertical impulse of $50kN$ *on the buoy.*

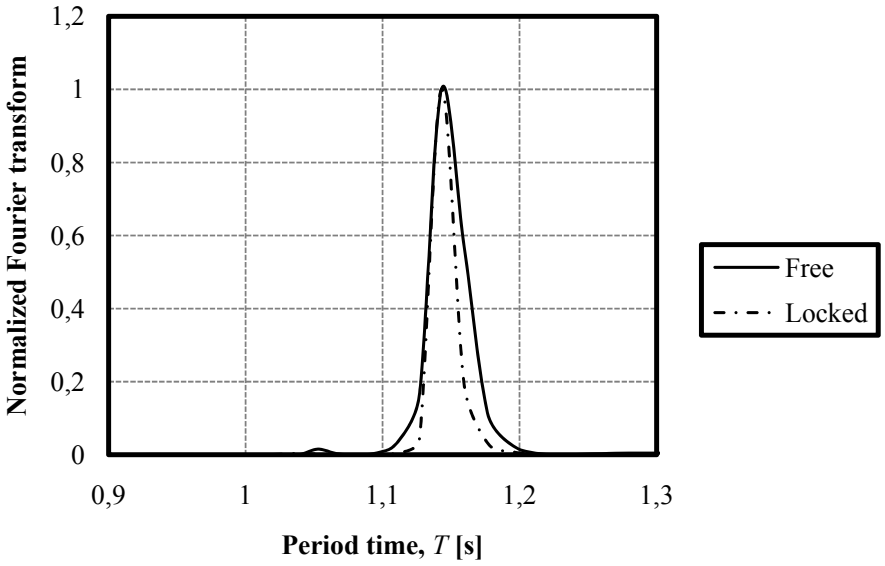

Figure 4.6: The Fourier transform of the tension force response in line number three. The load was in this simulation a vertical impulse of $50kN$ *on the buoy.*

From Figure 4.5 and Figure 4.6 the conclusion can be drawn that the eigenperiod of the second and third mooring legs, represented by the tension in line three, are unaffected by the piston configuration and that this period of $T_H = 1.11\ s$ is reflected onto the time response of the western mooring leg represented by the tension in line one. The opposite is however not true to the same extent as the eigenperiod of the tension in line number one is barely visible in the Fourier spectrum of line three. The tension force in line one is also much more dependent on the piston configuration and a slight shift in eigenperiod is visible as the inertia of the buoy is changed by the piston. It is the symmetry of the system which prevents this shift from occurring in line three. It can be explained by noting that a heave displacement does not change the force balance in the y-, or sway-, direction but it does so in the case of the surge response. When a vertical displacement of the buoy breaks the equilibrium of the mooring lines in the x-direction, a small but noticeable displacement can be seen. This slight displacement is enough to change the tension in the western mooring lines and therefore also alters the harmonic frequency. This also affects mooring leg two and three, but only the x-component of their resultant force.

The exact values of the eigenfrequencies or periods of the mooring lines are however irrelevant as these are varying with the tension force. The tension force is extremely varying in the simulations and it is therefore sufficient to note that the harmonic frequencies of the mooring legs are in the region of $1\ Hz$.

4.3.2 Surge and sway impulse

When the impulse is added in the x-direction the system shows signs of over-damping.

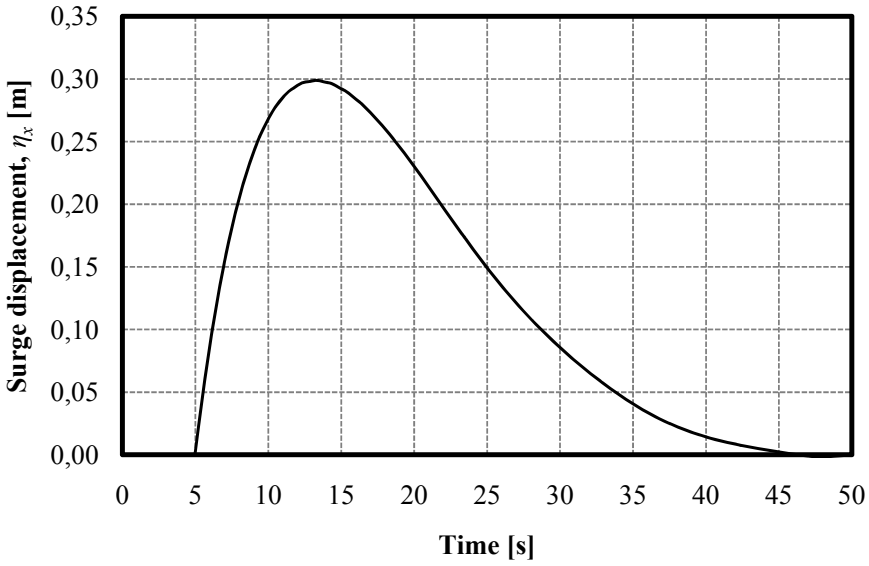

Figure 4.7: The time response of the surge displacement due to an impulse load of 50 kN *in the surge direction.*

The total period time of this motion would be in the region of $T = 40\ s$ as it takes $10\ s$ to obtain the maximum value, which corresponds to one quarter of a period. There is no risk of the surge motion creating any resonance problems as it is heavily damped and the harmonic period is four times larger than the longest of the common waves on site.

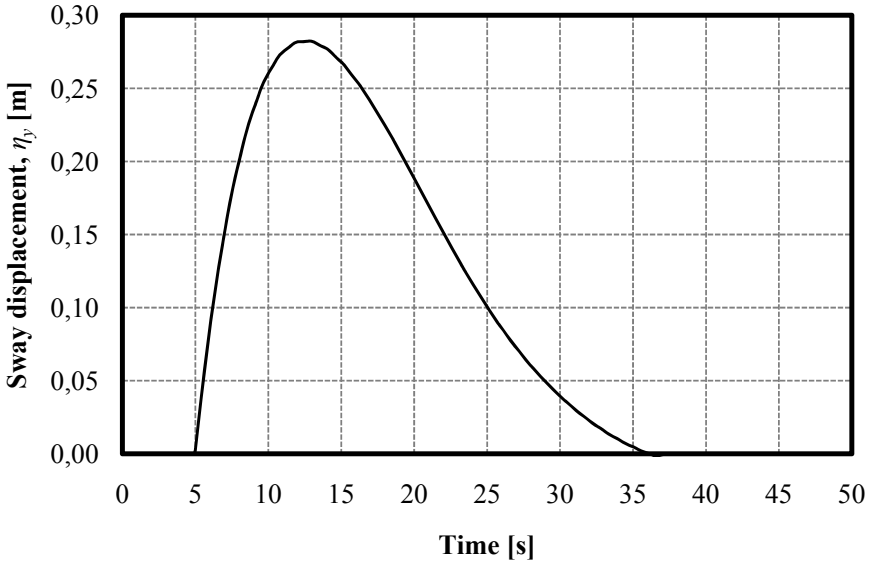

Figure 4.8. The time response of the sway displacement due to an impulse load of 50 kN *in the sway direction.*

There are two small but noticeable differences between Figure 4.7 and Figure 4.8. First of all the total period time of the sway motion is somewhat shorter than that of

the surge motion. Secondly the maximum displacement is also slightly smaller in the sway motion. Both of these results are due to the fact that the pre-tension in the horizontal mooring lines in static equilibrium is higher in the sway direction than in the surge direction. This accounts for both the increased harmonic frequency and the smaller amplitude of the motion response.

4.4 Time response

This section shows the typical results of a simulation with single frequency wave loading. The motion and the mooring force responses are presented in individual subsections.

4.4.1 Motion response

The buoy motion response to the default wave is seen in the figures below.

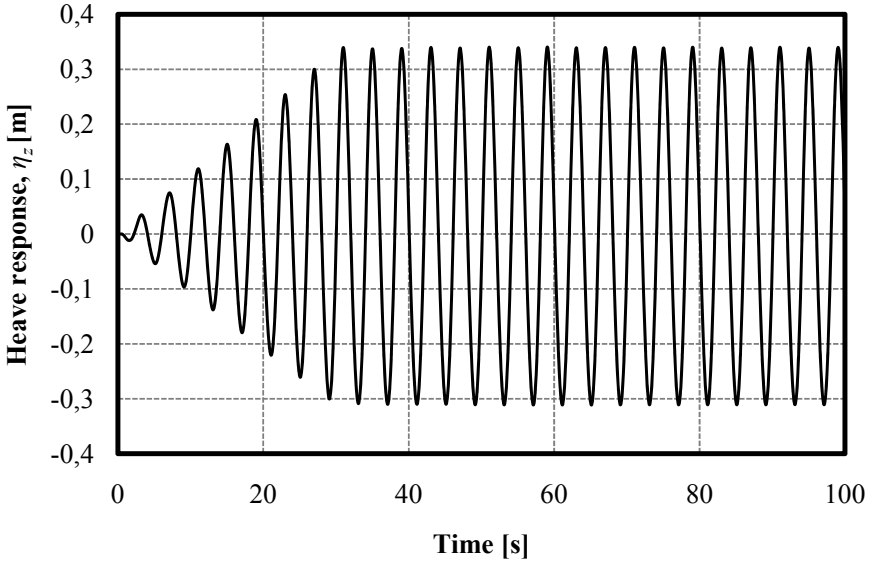

Figure 4.9: The heave response of the buoy as a result of the default wave simulation. The piston is here in the free configuration.

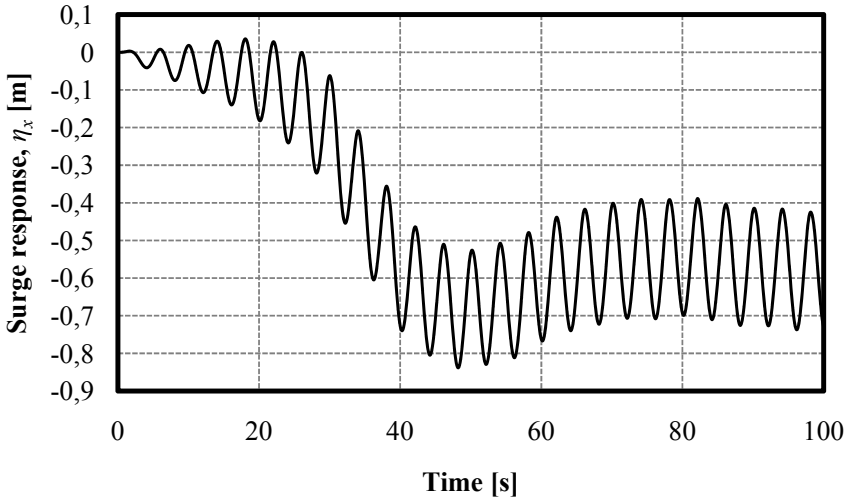

Figure 4.10: The surge response of the buoy as a result of the default wave simulation. The piston is here in the free configuration.

From Figure 4.9 the relative amplitude response can be computed as $\frac{|\eta_3|}{a} = \frac{0.32}{0.50} = 0.64$. This is a good measure of the impact the mooring system has on the heave motion. If, for instance the heave motion response should differ between different wave directions this difference can only come from the moorings as the buoy itself is completely axi-symmetric.

Figure 4.10 show the surge response to the default wave loading. This is a common scenario and it appears as if the system needs 90 s to stabilize and enter the regular phase of harmonic response without transients. This is however not the case when looking at the forces in the moorings.

4.4.2 Mooring forces

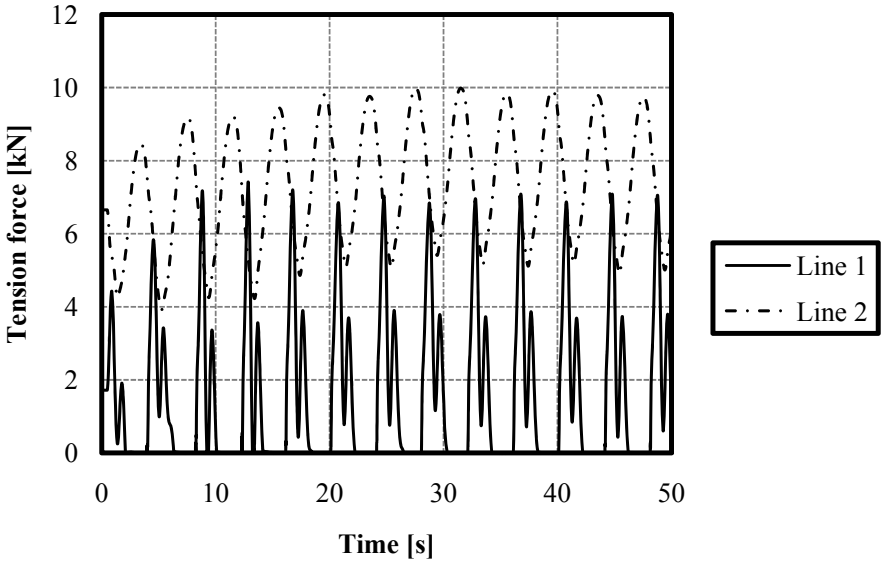

Figure 4.11: The time response of the tension force in line number one and two during the first 50 *s of simulation as a result of the incoming default wave.*

Figure 4.11 shows the transient period of the simulation where the system is adapting to the impact of the increasing wave. The period from $50\ s$ to $100\ s$ is said to be the regular phase in which all transients in the mooring forces are assumed to have died down.

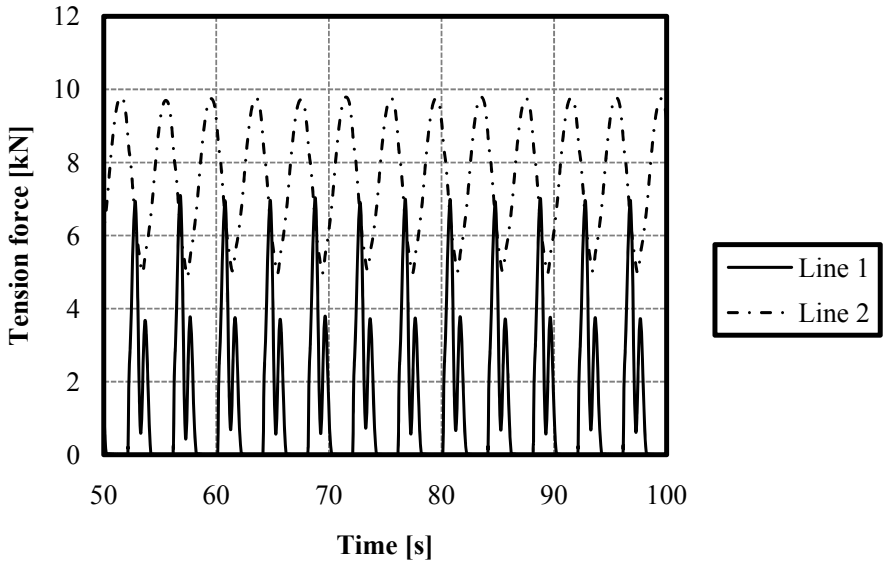

Figure 4.12: The time response of the tension force in line number one and two during the last 50 *s of simulation as a result of the incoming default wave.*

According to Figure 4.12 this categorization between transient and regular phases is a good assumption and it is validated by the same behaviour in line number three and four, see Figure 4.13 and Figure 4.14. The results of this chapter use the forces which are the maximum forces obtained in the regular time period of the simulation, i.e. between 50 and 100 *s* after the wave propagation was commenced.

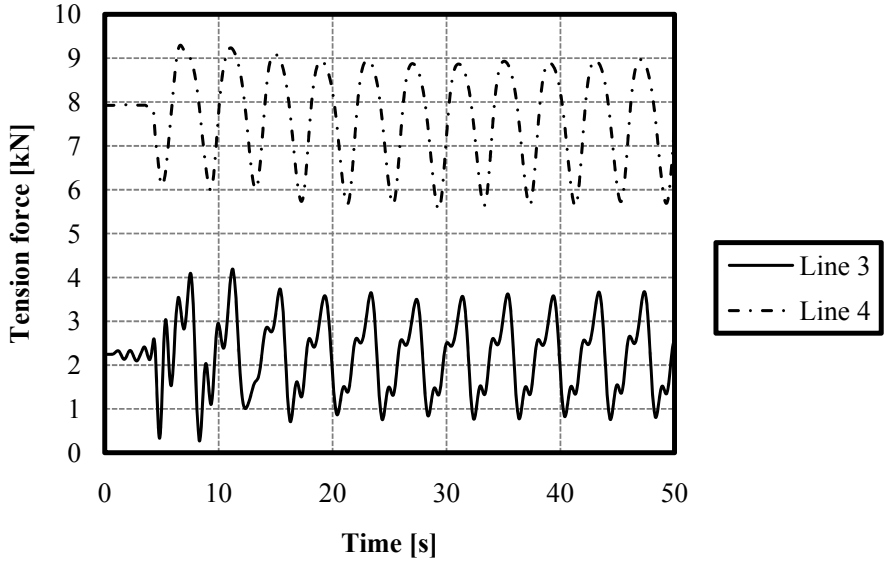

Figure 4.13: The time response of the tension force in line number three and four during the first 50 *s of simulation as a result of the default wave.*

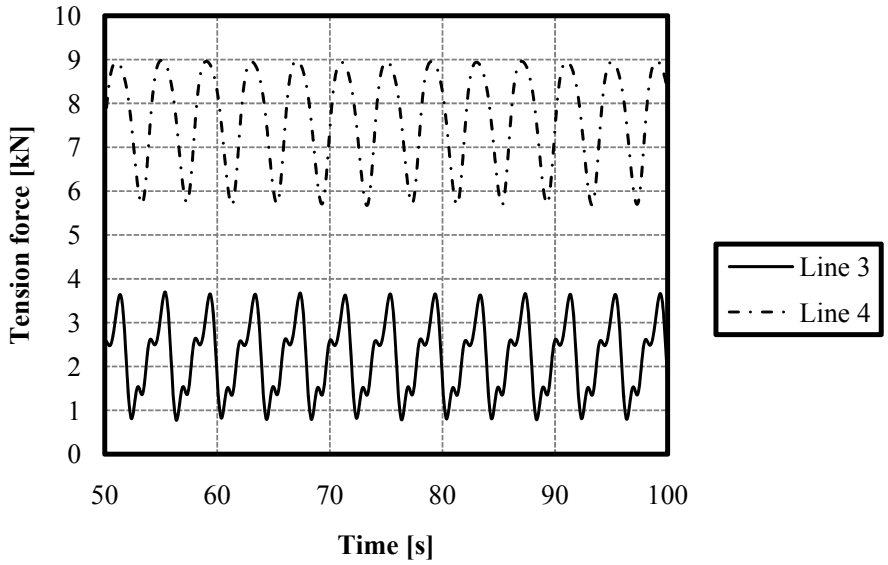

Figure 4.14: The time response of the tension force in line number three and four during the last 50 *s of simulation as a result of the default wave.*

The main difference between the tensions in the horizontal lines, line one and line three, is that line number three never slackens in this load scenario. The re-tightening of line one is the process which creates the most tension in the system. The slackening-tightening process is according to Bergdahl (2010) very complicated and it needs highly resolved models in time and space to model correctly. The predictions of the program about the magnitude of the maximum forces are therefore relatively uncertain as the low resolution in space is a potential source of error. It has fallen

outside the scope of this thesis to study this phenomenon in more detail and it is therefore just briefly mentioned here.

The main oscillation of the mooring line tensions is naturally at a period time equal to that of the loading scenario, but as seen most clearly in Figure 4.12, but also in Figure 4.14, there is a perturbation oscillation of about $T = 1\ s$. This is the same as seen in the impulse investigation and is the eigenperiod of the mooring legs with a relatively stationary buoy.

4.5 Wave direction

The mooring system is not completely symmetrical in the xy-plane, and it is therefore more sensitive to loading from certain directions. To find the critical angles of wave propagation, waves coming from the first two quadrants of the xy-plane (from West through South to East) have been allowed to affect the system. See Figure 3.3 and (3.1) for used angles of propagation, θ_w.

4.5.1 Motion response

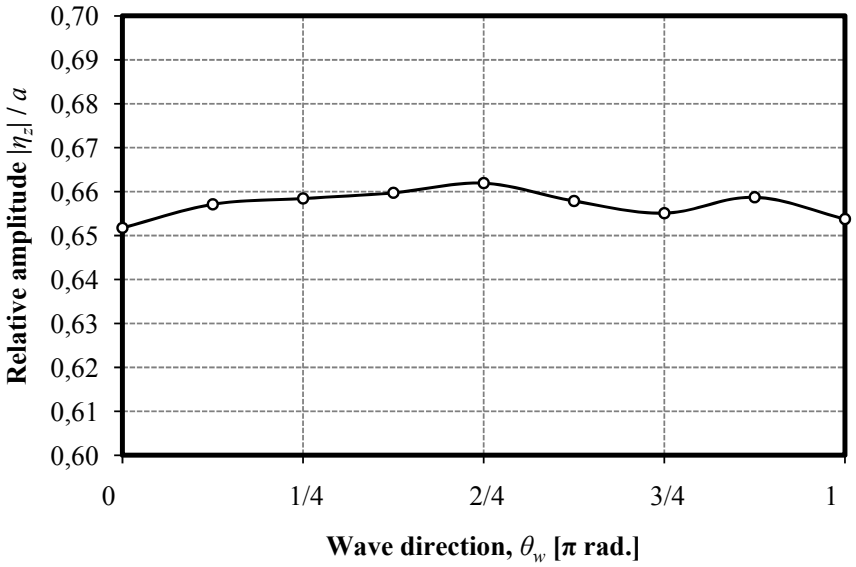

Figure 4.15: The variation of the relative amplitude response as a function of the wave direction.

There is a slight difference in the relative amplitude of the buoy between the different directions of wave propagation in Figure 4.15. The maximum is reached in southern or northern seas, but the scale of the difference is insignificant compared to other factors determining the relative amplitude, such as period time of the wave. Even so the results clearly points out that the mooring forces are affecting the heave motion to some extent at least.

4.5.2 Mooring forces

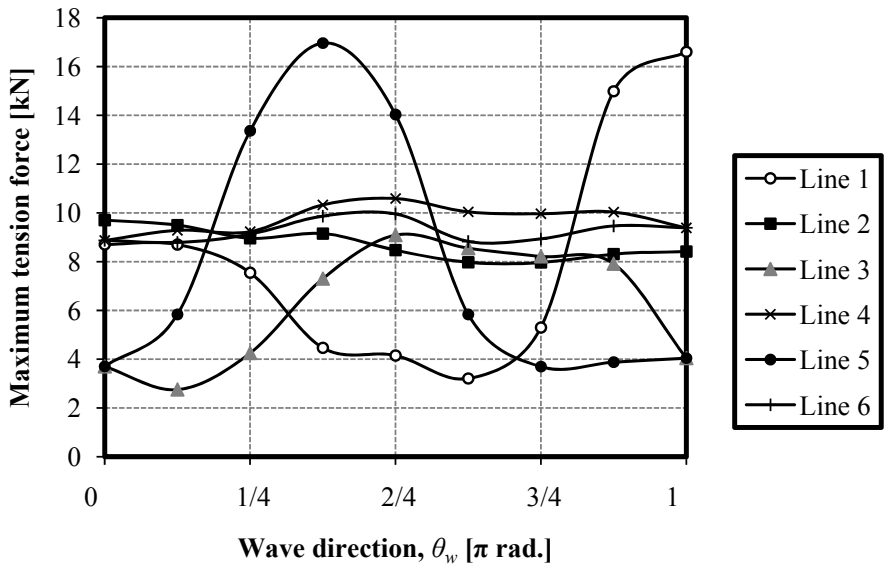

Figure 4.16: The influence of wave direction on the maximum tension in the mooring lines.

It is clear that it is foremost the horizontal lines that are strongly affected by the direction of the waves. This is natural, as the vertical line tension would be completely unaffected by the direction if there were no horizontal lines, which is why any change in their maximum tension is only a response to the change in the horizontal line tension. The most remarkable result however, is that the maximum tension seem to be on the mooring line of the lee side of the incoming wave. This is the case for both line number five and number one, the latter of which has a clearly higher maximum tension value in easterly, $\theta_w = \pi$, waves than in westerly, $\theta_w = 0$, waves. The case $\theta_w = 0$ is in fact the default wave, and the time response of line one and two can be seen in Figure 4.12.

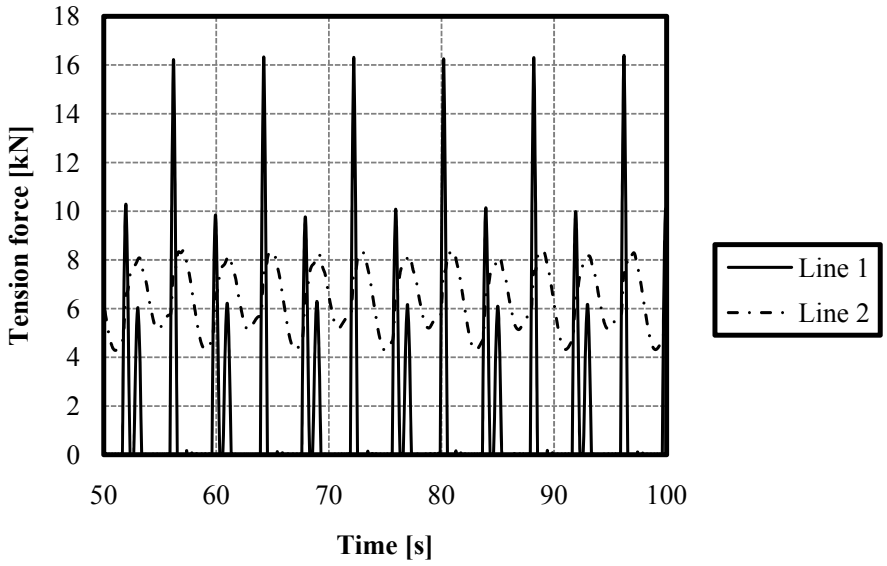

Figure 4.17: The regular time response of line number one and two as a result of the incoming default wave with $\theta_w = \pi$.

Figure 4.17 shows a similar behavior as Figure 4.12 at every other period. The maximum value is obtained by the intermediate single peaks of the time response, which are approximately 50% higher in magnitude.

The difference between the response in the mooring force between the two propagation directions concerns the vertical line number two. In western waves, the buoy and the floater number one are both drifting slightly to the east, as a consequence of the wave loading. The floater motion is then restrained by the tension force in line number two which is facing the waves. In the easterly waves, $\theta_w = \pi$ rad, this force is instead working as an added force to the wave load drift force and the average distance, and the relative velocity at the moment of re-tightening are both increased.

4.6 Wave period

The most complex behaviour of the mooring system comes when a sweep is made over different wave periods.

The waves in this investigation are all plane waves propagating along the negative x-axis, $\theta_w = 0$. This means that the projection of line number one onto the wave direction is its entire length, $L_1 = 15$ m, whilst line three and five only show a fraction of their length, $L_3 \cos\left(\frac{155}{2}\right) = 3.24$ m, see Figure 3.2. Thus a wave with $\lambda = 15$ m should result in that the buoy and floater one are moving in phase with each other. Table 4.2 show the wavelengths of the different waves, and the phase shift due to the geometry between the buoy position and float one and two respectively.

Table 4.2: The k-values and wavelengths of the different waves used in the simulations. ψ_{b-f_1} and ψ_{b-f_2} are the geometrical phase shifts between the buoy and floater one and two respectively.

Period time, T [s]	k-value [m^{-1}]	λ [m]	ψ_{b-f1} [rad]	ψ_{b-f2} [rad]
2	1.006075	6.245245	2.524754	-3.0235
2.25	0.794923	7.904143	-0.64252	2.57555
2.5	0.643890	9.758166	-2.90802	2.086203
2.75	0.532138	11.80744	1.698885	1.724128
3	0.447145	14.05178	0.423989	1.448749
3.25	0.380997	16.49143	-0.56823	1.234429
3.5	0.328513	19.12614	-1.35549	1.064381
3.75	0.286173	21.9559	-1.99059	0.9272
4	0.251521	24.98076	-2.51037	0.814929
4.25	0.222801	28.20088	-2.94117	0.721875
4.5	0.198733	31.61622	2.980994	0.643895
4.75	0.178365	35.22656	2.675475	0.577902
5	0.160973	39.03254	2.414594	0.521552
6	0.111816	56.19218	1.67724	0.362285
7	0.082356	76.29299	1.23534	0.266834
8	0.063656	98.70531	0.95484	0.206246

4.6.1 Motion response

4.6.1.1 Relative amplitude

Figure 4.18 shows the heave response of the buoy as a function of wave period time. Simulations have been made with both the piston configurations because of its great effect on the harmonic period.

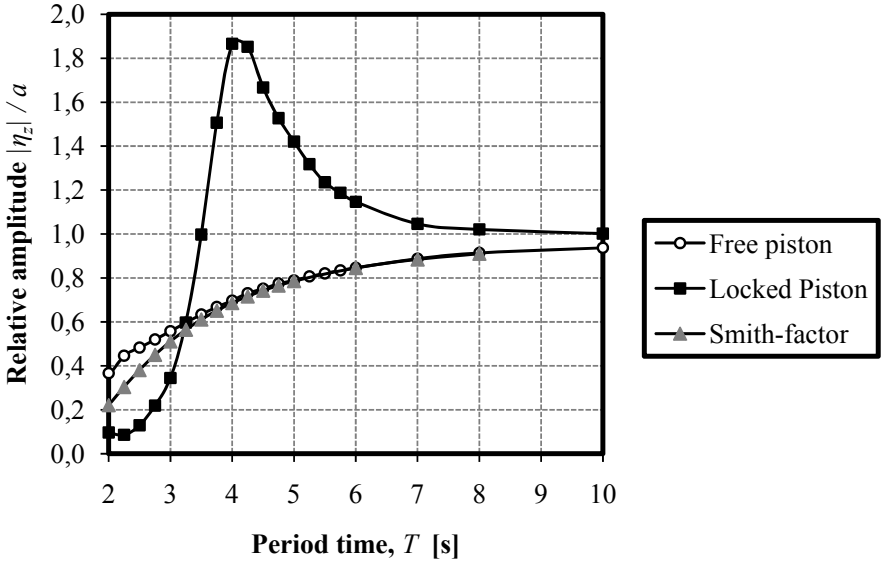

Figure 4.18: The relative amplitude of the buoy response in heave as a function of period time of the wave.

The value of the relative amplitude is strongly dependent on the period time of the oscillations. Normally it is resonance effects that are most dominant, but for short wavelength the Smith-factor, $\frac{\cosh(k(H-z_b))}{\cosh(kH)}$ in the velocity potential of equation (2.7), makes a big difference. It is strongly dependent on the wave number k and the draught, $z_b = 1.5$ m which is the distance from the still water surface to the bottom of the buoy. As the resonance frequency for the buoy with free piston is so high the Smith-factor strongly dampens the relative amplitude response at resonance. However, one must remember that the free piston configuration can not be used to generate any power. As the extra damping from the piston force is added, the eigenfrequency will decrease, as will k for the resonance wave. Thus the Smith-factor will not be so dominant when the buoy is actually in operation, as the graph for the locked piston in Figure 4.18 shows.

4.6.1.2 Phase lag

The motion response of the buoy is not necessarily in phase with the motion of the water particles. It will move with the same frequency but might be shifted, or lagging, in phase. The magnitude of this phase lag is frequency dependent and goes toward zero as the frequency goes to zero, so that for long wavelengths the buoy and water oscillates in phase.

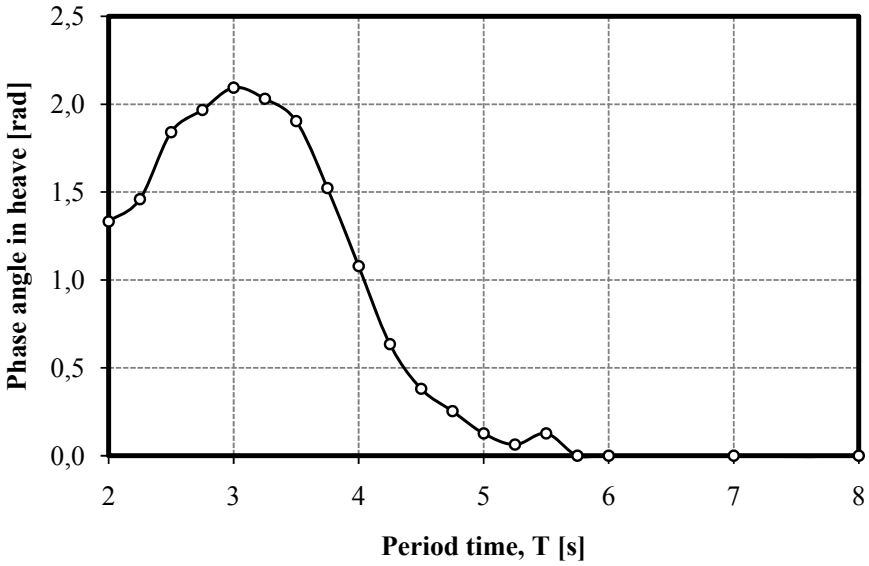

Figure 4.19: The phase angle between water and heave motion of the buoy as a function of period time of the waves. The results are from simulations with locked piston configuration.

The maximum phase shift in Figure 4.19 is at the wave period of 3 s. The results confirm the theoretical predictions in the sense that the long period response goes to in-phase movement and that the maximum phase shift is at a period time which is somewhat shorter than the eigenperiod, see BERGDAHL (2009).

4.6.2 Mooring forces

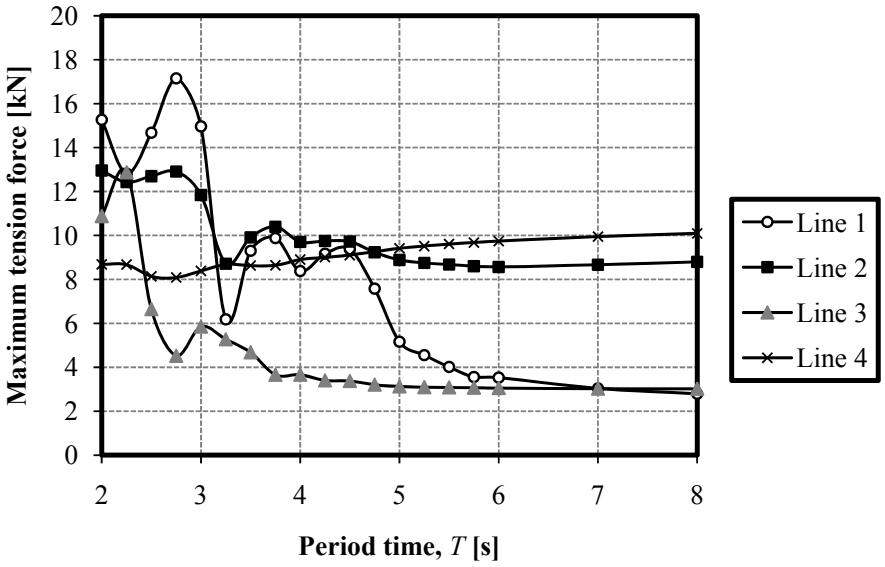

Figure 4.20: The maximum tension force variation in the mooring lines as a function of the period time of the incoming wave.

Three dips are seen in the tension force of line number one in Figure 4.20. The first is at $T = 2.25\ s$, the second at $T = 3.25\ s$ and the last at $T = 4\ s$. There is also a clear transition into long wavelength response after about $T = 6\ s$ which is connected to that the maximum phase lag between buoy and float is negligible as the wavelength is increased beyond $\lambda = 2L_1$, which is seen both in Table 4.2 and Figure 4.19. Here the effect of the acceleration and velocity of the water particles is decreased.

The overall decreasing form of the graphs of the horizontal lines is caused by the decrease in relative speed at the moment of re-tightening of the line; compare with Figure 4.12. As the simulations have the same wave amplitude, it is only natural that the force response is decreased with the decrease of energy content of the wave.

As the heave response at resonance was so limited in the case of the free piston, it is instructive to investigate the mooring force response in case of the locked piston configuration.

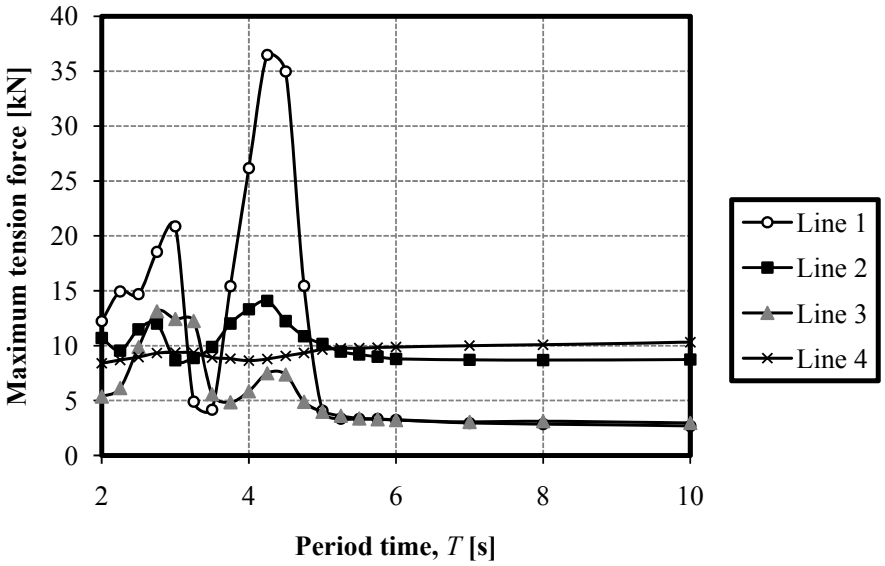

Figure 4.21: The maximum mooring force response as a function of period time of the wave in the case of locked piston position.

The maximum tension force in Figure 4.21 is naturally higher than the equivalent force with free piston. The forces are the highest at resonance, which is only natural as the displacements and velocities of the buoy then is at a maximum.

The tension force reaction to variation of period time is not easily interpreted. It is the result of a combination of several different factors. Of course the phase lag due to the geometrical distance between the floater and the buoy and the phase lag of the buoy itself is important. The floaters themselves are also affected by the waves, and are due to their small inertia subjected to larger displacements in the horizontal direction than the buoy is. This motion is also lagging in phase, but as seen in Section 4.3 the eigenfrequency of their motion is in the order of $1\,Hz$ and the corresponding phase lag curve is thereby shifted accordingly, and the long wavelength behaviour is reached at a shorter period time. Finally, the mooring forces themselves naturally also affect the relative motions of the buoy and the floaters. Figure 4.22 shows the typical surge motions of the buoy and float number one.

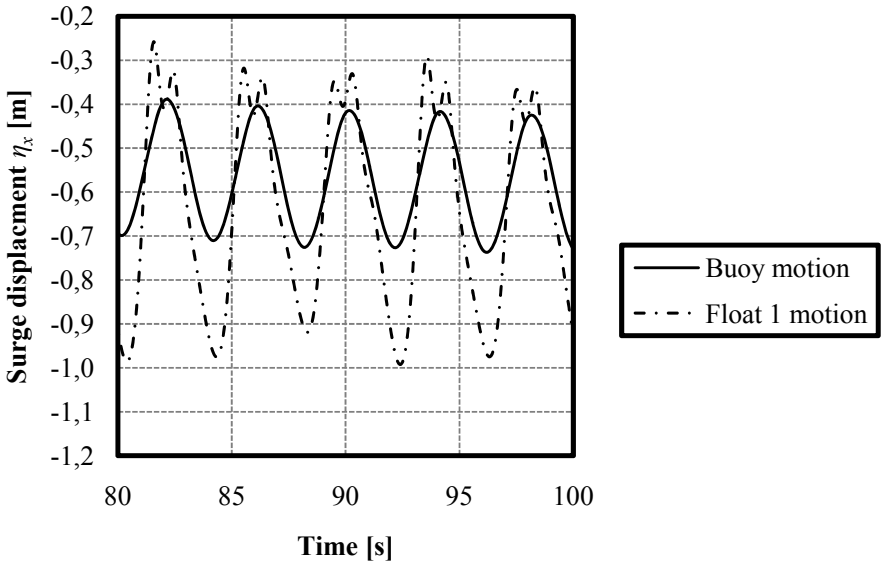

Figure 4.22: The surge motion of the buoy and float number one with respect to time. The results come from the simulation of the default wave.

It is clear from Figure 4.22 that the mooring force dominates the motion of the floater as soon as the distance between buoy and float is sufficiently large. The dashed curve in Figure 4.22, the floater motion, below the buoy motion represents the undisturbed oscillation of the floater only moored by line number two. As the magnitude of its displacement passes that of the buoy, the motion is damped by the horizontal mooring cables and a slight oscillation at its eigenfrequency can be seen.

4.7 Wave amplitude

4.7.1 Motion response

Looking at the heave motion the relative amplitude shows little dependence on the wave amplitude.

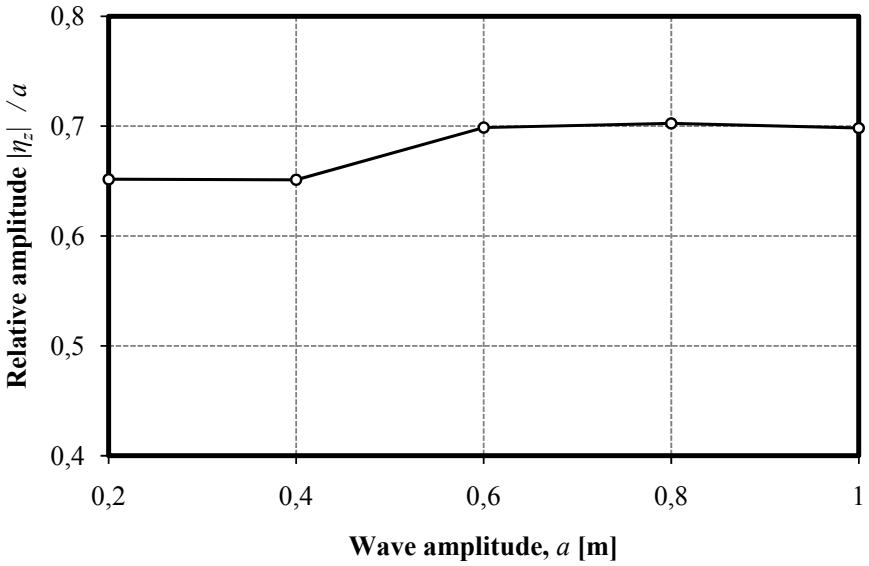

Figure 4.23: The change in relative amplitude as a function of wave amplitude a.

4.7.2 Mooring forces

The wave amplitude is in general increasing the maximum tension force.

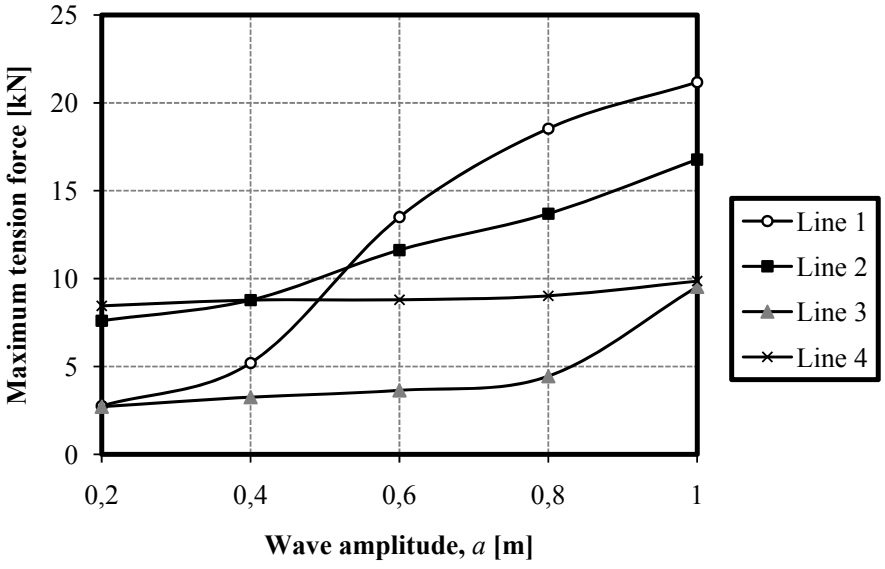

Figure 4.24: The maximum tension force as a response to the default wave with varying amplitude from $a = 0.2\ m$ to $a = 1\ m$.

The fact that line number one and two are the most affected by an increase in wave amplitude is related to the direction of the wave. The strongest effect is seen when the

horizontal projection of the mooring line is parallel to the horizontal flow direction, in this case this effect is strongest for the lines of the western mooring leg.

4.8 Current speed

The effect of the current speed is investigated by looking at its effect on the static equilibrium of the system. The mooring forces are computed as the static forces without the addition of waves, and the resulting offsets of the buoys equilibrium position are studied. The current direction has in these simulations been chosen to $\theta_c = 0$ rad.

4.8.1 Motion response

The quadratic nature of the drag force, see (2.3), reveals itself in Figure 4.25, as this is the only term that changes in the simulations in the absence of waves.

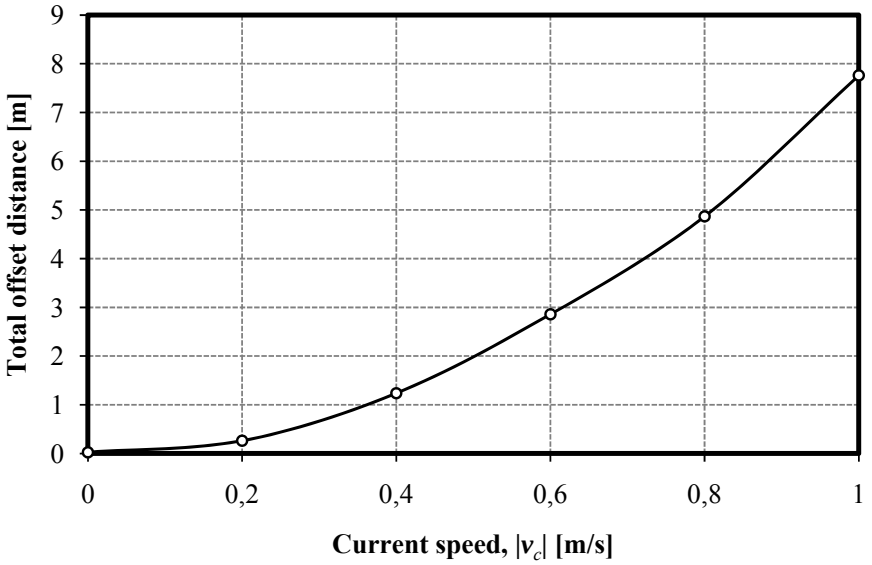

Figure 4.25: The stationary offset distance of the buoy as a function of the current speed. The simulations were made using $\theta_c = 0$ rad.; i.e. the current direction of motion was from west to east.

The offset magnitude increases with the current, and it is not a linear dependence. It is in fact dependent on the responsive forces from the mooring system, which are in turn dependent on the floater response to the current load, and also the drag coefficient, which changes drastically as the transition from laminar to turbulent boundary layer flow, is made. The result of Figure 4.25 are however clear, and the dominating term is obviously the current speed.

4.8.2 Mooring forces

The evolution of the mooring forces in the case of a western current of varying speed is seen in Figure 4.26 below.

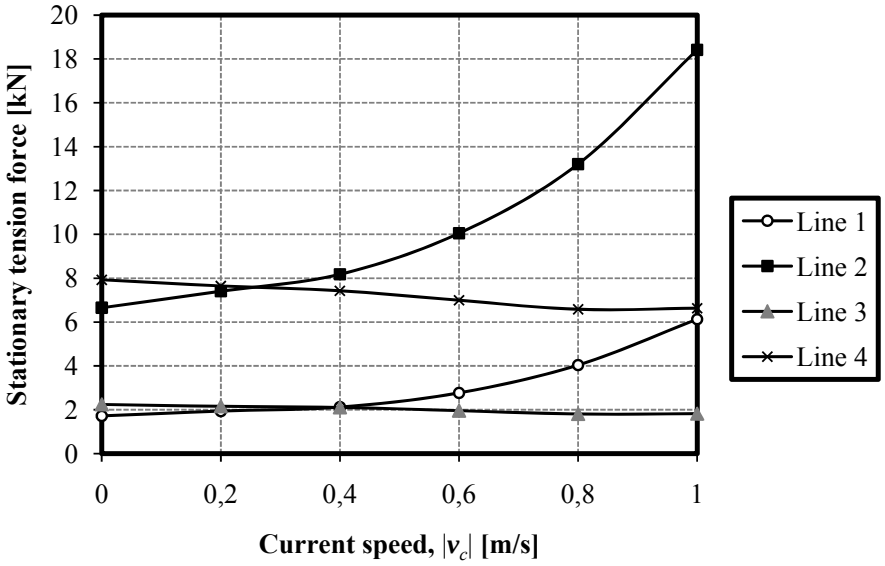

Figure 4.26: The stationary mooring forces in the mooring lines as a function of current speed. The simulation was made without any wave addition, and the current direction was $\theta_c = 0\ rad$.

It is clear that the load due to current is most critical for the vertical lines. Again the quadratic appearance is seen. It is also apparent that mooring leg one, consisting of line one and two, is more affected as the current is directed in the same direction as the pre-tension of it.

4.9 Current direction

The impact of the direction of the current is investigated using the maximum current speed of $|\boldsymbol{v_c}| = 1\ m/s$ and otherwise calm water. The current directions are, as mentioned in Section 3.2.3, taken from the first and second quadrants of the xy-plane. As the mooring system is symmetrical with respect to the x-axis, nothing new can be gained from simulation of currents attacking the buoy from quadrant three or four.

4.9.1 Motion response

As the buoy and the mooring system are subjected to a water current, the equilibrium position will be changed as the force balance is shifted due to the drag force on the submerged structures. Figure 4.27 shows the equilibrium positions of the buoy for the different simulated current directions.

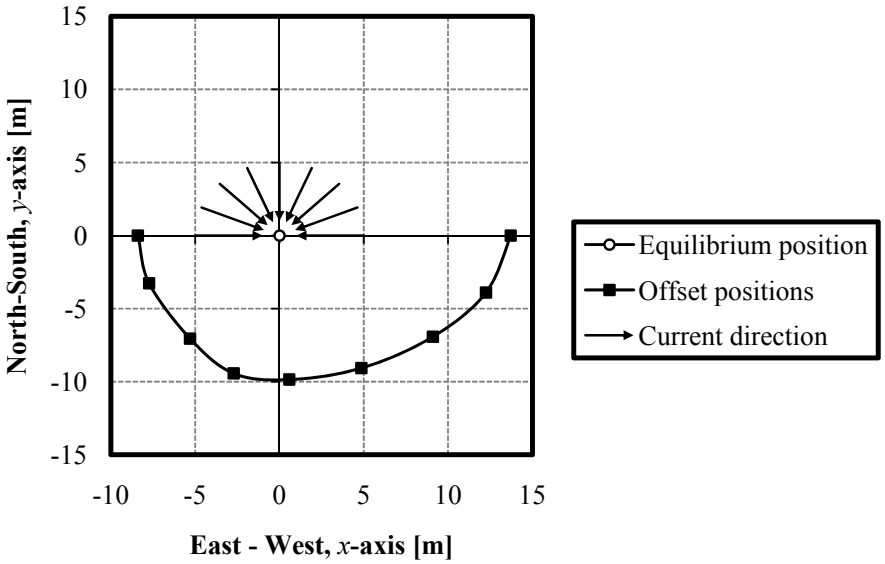

Figure 4.27: The offset of the buoy due to a current of $|\boldsymbol{v}_c| = 1m/s$ coming from different directions.

From Figure 4.27 it is clear that the mooring system is designed to be the most rigid when subjected to load from the west. One can also see the break in symmetry when looking at the offset corresponding to a sea current from the south. It is not directly north of the equilibrium position but has drifted slightly to the west, the positive x-direction. Another way to evaluate the sensitivity of the offset to the current direction is to look at the norm of the displacement. Using the same data as in Figure 4.27, one can clearly see in Figure 4.28 how the buoy offset increases with the current direction's deviation from the x-, or westerly direction.

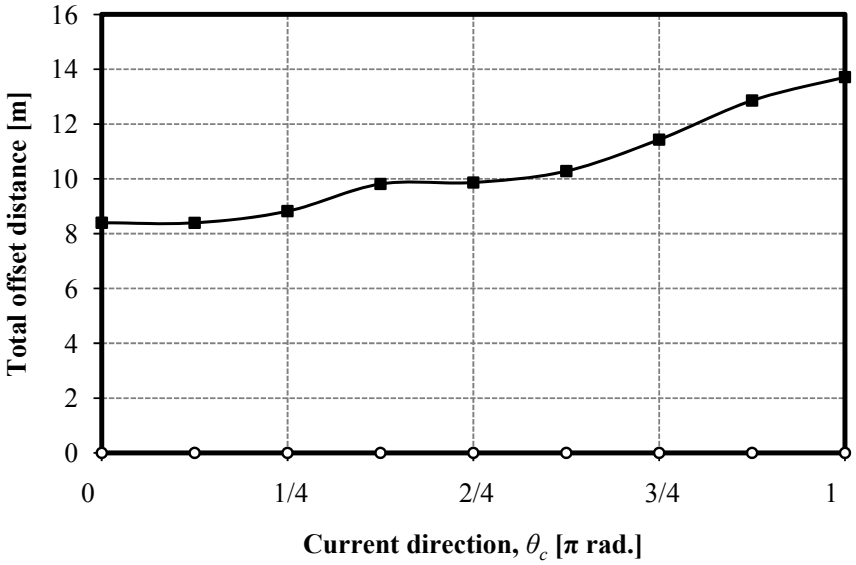

Figure 4.28: The equilibrium offset distance of the buoy as a function of sea current direction.

4.9.2 Mooring forces

The shift in equilibrium position is of course accompanied by a corresponding shift of the stationary mooring forces. This affects the tension forces in both the horizontal and the vertical lines.

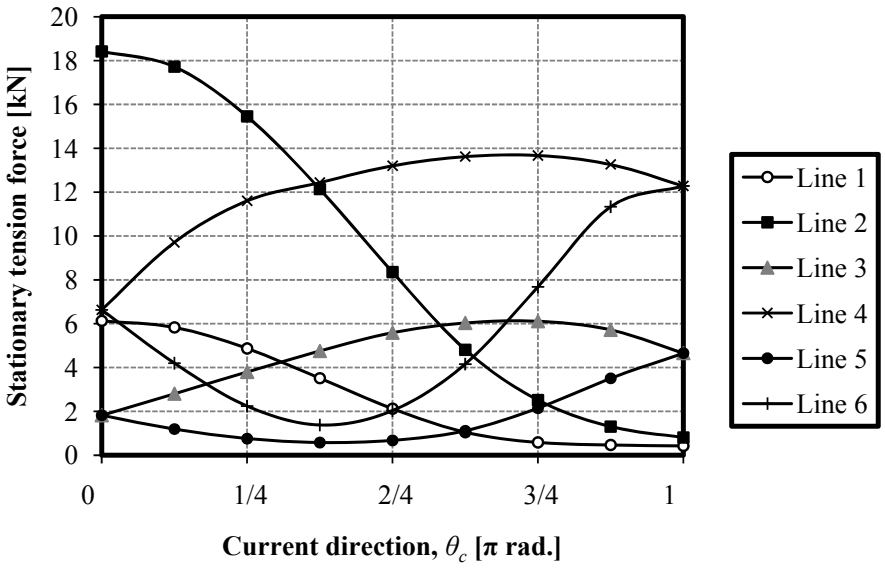

Figure 4.29: The variation of the stationary tension force as a function of current direction. Here $|\boldsymbol{v}_c| = 1\ m/s$ *in otherwise calm water.*

It is clear from Figure 4.29 that the worst strains are in the vertical lines, as these have one end fixed to the anchor point whilst both of the endpoints of the horizontal lines are moving in response to the increased current. There is also a clear tendency to reach the maximum and minimum tension in the mooring lines when the current direction is parallel to the horizontal projection of the line.

4.10 Irregular waves

As mentioned in Section 2.4, waves at sea are not in reality composed of a single frequency, but are instead the superposition of many different waves. They can have varying amplitude, frequency and direction of propagation. Waves synthesized by a JONSWAP spectrum with peak amplitudes for $T_m = 4$ s, $H_s = 1.5$ m, with a directionality criteria of cosine square type around the x-axis and the use of random phase has been used in the following simulations. See Section 2.4 for more detailed information about the wave generation. It was seen in Section 4.6 how the locked piston configuration of the buoy gave a larger amplitude response in heave than the free piston did. Therefore the locked configuration has been used in the simulation of the response to irregular wave loading.

The synthesized wave used in this investigation is of the following appearance, for future reference.

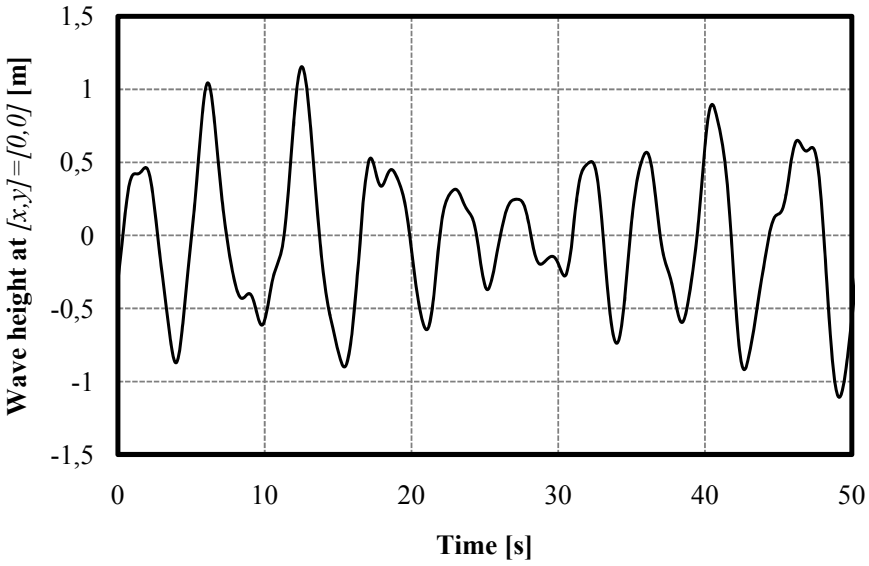

Figure 4.30: The time evolution of wave height of the irregular wave used in the simulations at $[x, y] = [0,0]$.

4.10.1 Motion response

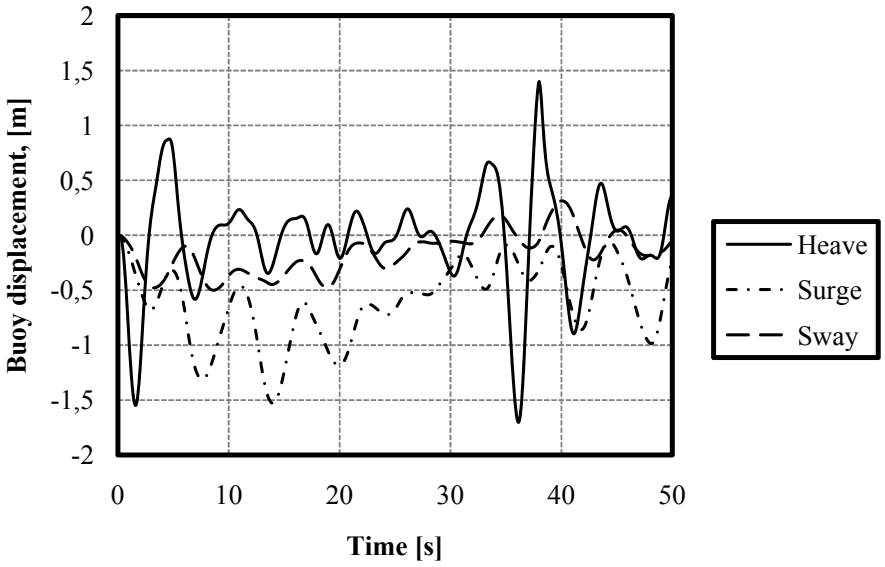

Figure 4.31: The motion of the buoy in irregular waves as a function of time. The piston position has been free in this simulation.

The buoy follows the irregular pattern of the waves in heave, but is of course also affected in the surge and sway direction. The surge has a larger maximum displacement than the sway as a consequence of the directionality criteria in Section

2.4.3. The displacements are not dangerously large and do not point at any critical phenomena that arise when looking at irregular waves.

4.10.2 Mooring forces

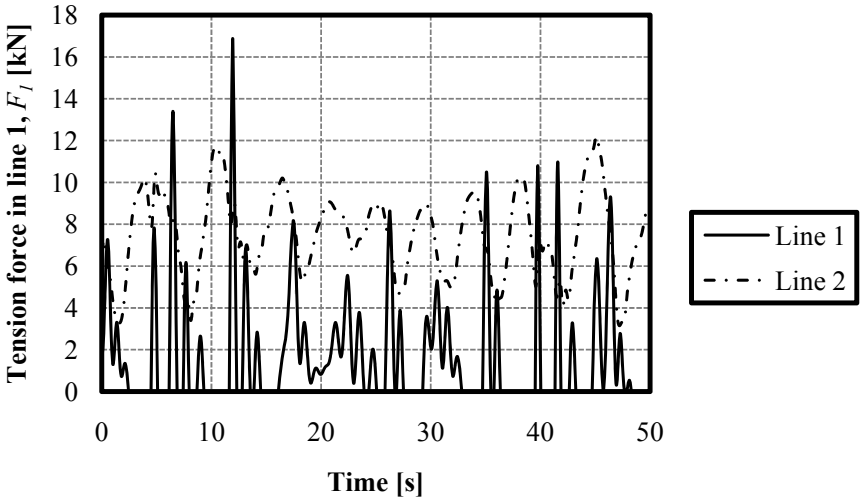

Figure 4.32: The mooring force response in the western mooring leg to an irregular wave loading scenario of $T_m = 4$ s, and $H_s = 1.5$ m. The piston position has been free in this simulation.

As Figure 4.32 shows, the mooring forces are by no means larger than in the corresponding regular loading scenarios studied in the previous subsections of this chapter. The actual response varies of course strongly with the energy and form of the irregular wave, but the order of magnitude is the same as the single frequency loading of the same mean period and wave height.

4.11 Marine growth

In a marine environment one cannot assume that the buoy and the lines will be unaffected by the marine life. Here the growth on the system has been simulated by choosing the marine growth curve in Figure 3.5, for the approximation of the drag coefficient, and the mass and diameter of the mooring lines have both been doubled.

The same irregular wave as in 4.10 has been used to study the effect of marine growth, and a comparison between the responses of the system with and without the added growth has been made.

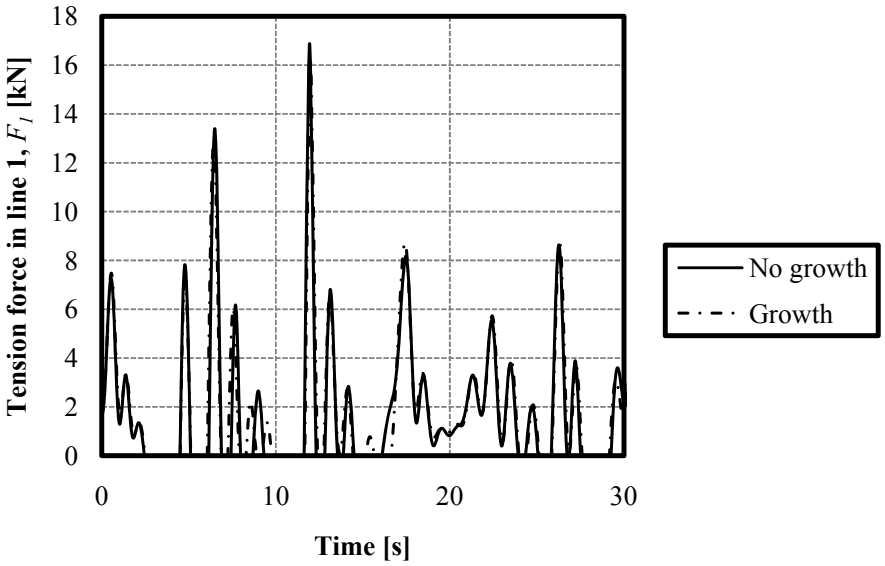

Figure 4.33: The effect of marine growth on the tension force in line number one. The piston position has been free in this simulation.

There is a small, but basically insignificant effect of heavy marine growth on the mooring lines and the buoy pipe. It is clear from Figure 4.33 that the tension forces remain basically unchanged by the added mass and diameter of the lines. There are some phase shifts in the responsive forces which are connected to the surge and sway response of the buoy and how this is affected by the change in drag coefficient, C_D.

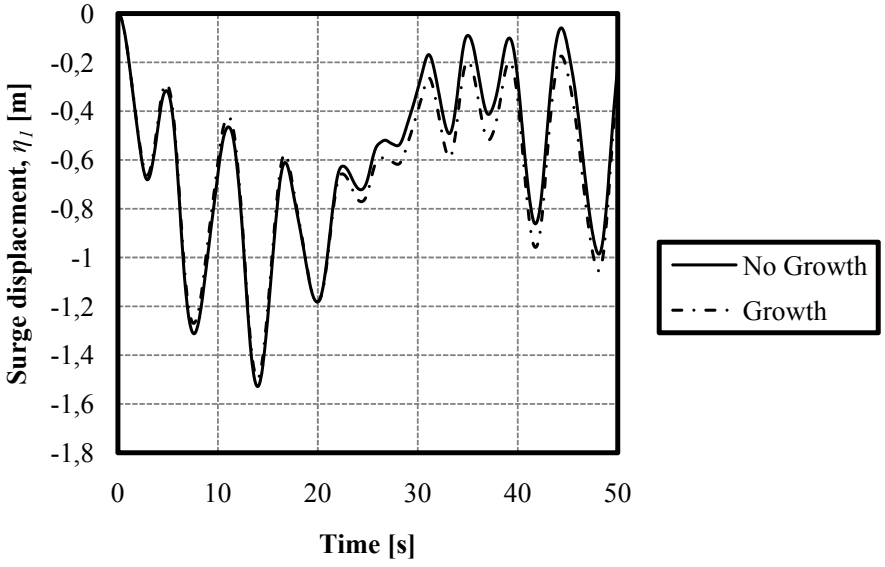

Figure 4.34: The surge displacement difference between simulations in irregular waves with, and without marine growth. The piston position has been free in this simulation.

The surge displacement in Figure 4.34 is somewhat changed, and the response is generally somewhat larger for the growth covered surface, which could be expected.

4.12 Wear of the mooring lines

The simulations have so far been concentrated on the response of the new mooring lines. The wearing of the line affects the entire system, but of course the mooring forces in particular. The system becomes more rigid as the mooring lines loose elasticity, see Figure 3.8. This results in that the default pre-strain of line number two corresponds to a stiffer system at equilibrium for an old line than for a new.

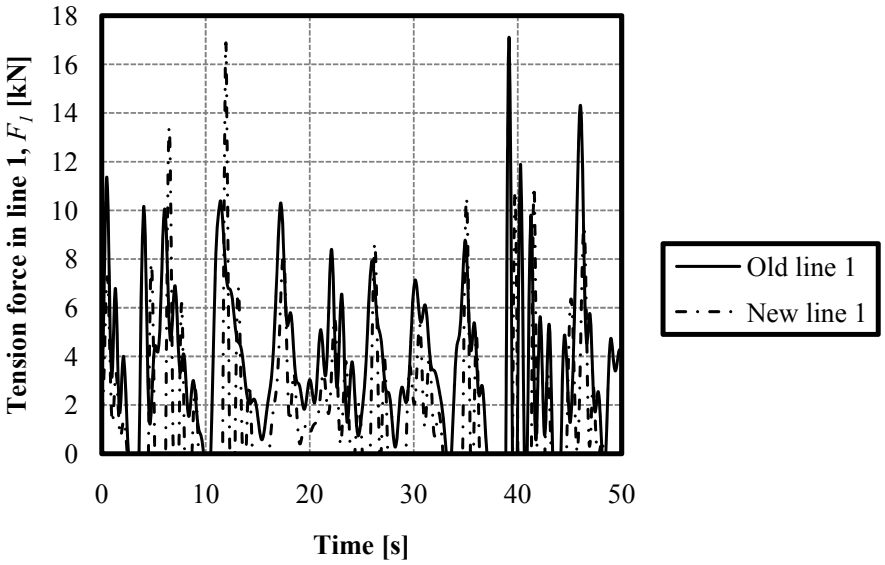

Figure 4.35: A comparison between the mooring force responses of line number one with old and new mooring line material. The loading scenario was that of the same irregular wave as was used in Section 4.10.

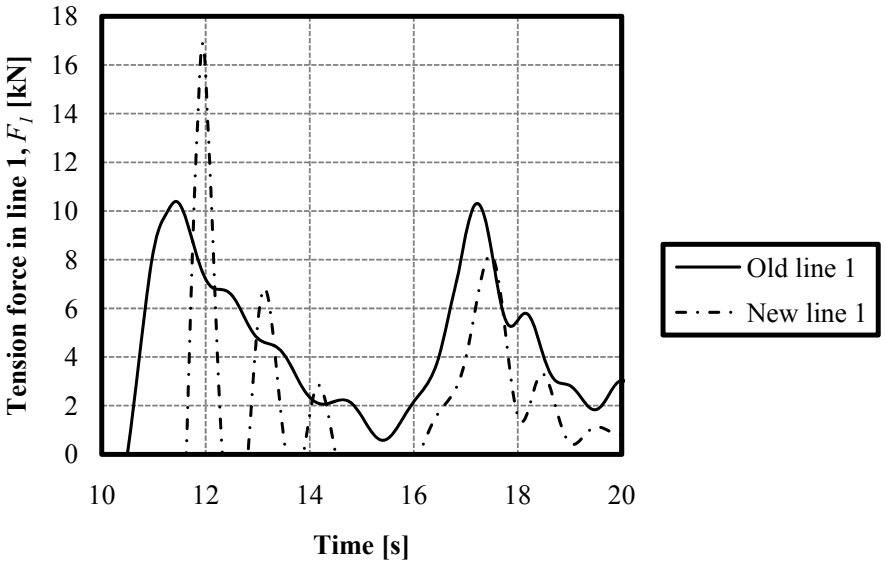

Figure 4.36: A comparison between the mooring force responses of line number one with old and new mooring line material. The figure shows the response between 10 *and* 20 *s of simulation and the loading scenario was that of the same irregular wave as was used in Section 4.10.*

The results show how the maximum force of the system still is in the same order of magnitude, but do not occur at the same time in the simulations. Figure 4.36 shows the time period surrounding the time of the maximum force of the new line, and it shows how the number of slacking times of the line is decreased by the stiffer behaviour of the line. The stiffer system seems to work beneficially on the mooring force response.

There is also a difference between the two surge responses of the simulations.

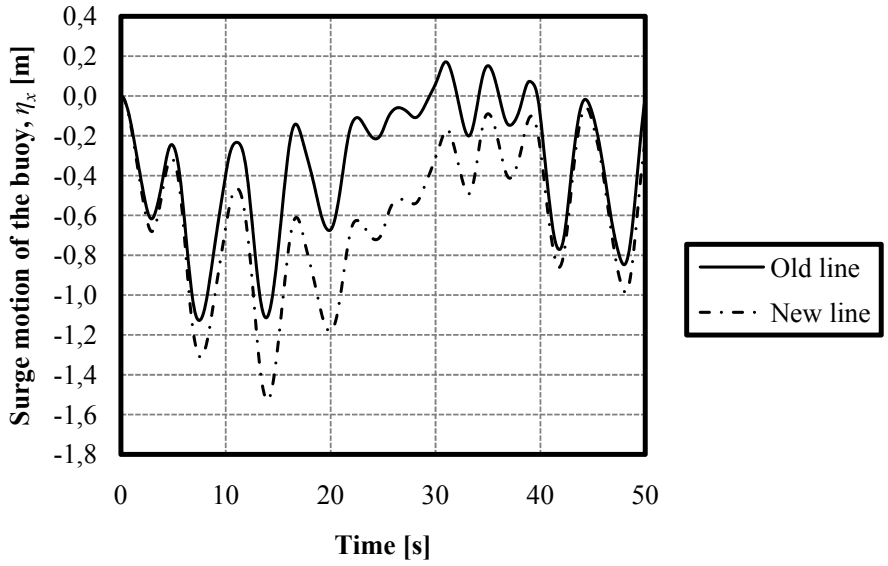

Figure 4.37: The surge motions of the buoy in the case of old- and new mooring lines respectively.

The new mooring line configuration clearly allows a larger buoy displacement than the old one, as seen from Figure 4.37. This and the decrease of slacking occasions of the mooring line make the investigation of increased pre-tension in the system highly interesting, as this might be the answer to the position mooring problem that tries to minimize the surge motion without affecting the heave of the buoy.

4.13 Position mooring

The aim of this mooring solution geometry is to keep the buoy stationary in the horizontal direction, and at the same time allow it to oscillate freely in the vertical direction. As seen in Figure 4.28 the buoy is still drifting significantly, and it is therefore interesting to see if the maximum drift distance can be decreased by increasing the pre-set tension in the mooring lines.

4.13.1 Motion response

From before it is known that the current is the factor that causes the largest offset of the buoy. Here the norm of the buoy's stationary displacement as a function of the strain in line number two, ϵ_2, in calm water is studied. The loading scenarios have been composed of the same current speed and current directions as in Section 4.9.1.

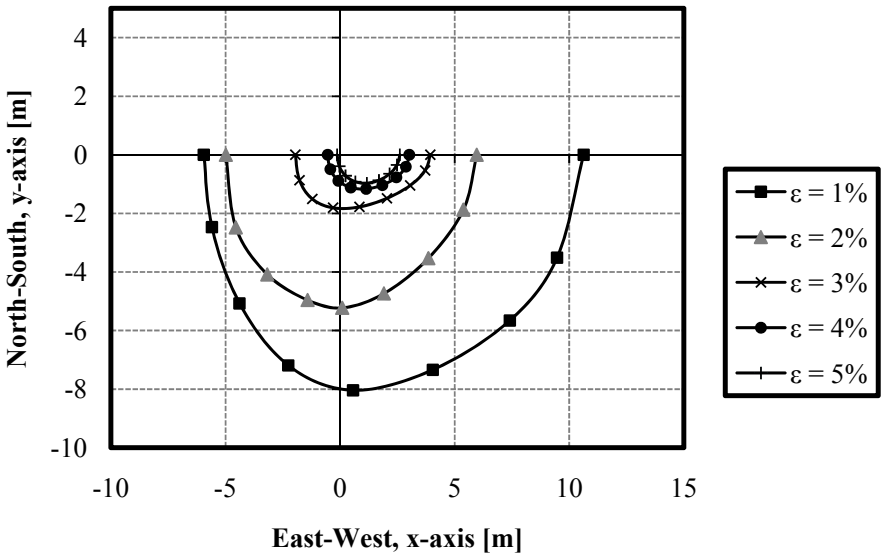

Figure 4.38: The effect of an increased strain of line number two at equilibrium on the equilibrium position of the buoy in maximum current speed. The same directions and speed as in Figure 4.27 have been used.

Here the graph representing $\epsilon = 1\%$ is the same as in Figure 4.27. The increased strain, and in consequence the increased tension force, gives a clear beneficial impact on the offset position of the buoy in maximum current. An increased tension gives a more rigid system, which is definitely more desirable in a potential wave power park setting where the need to restrict the horizontal movement of the buoy is very critical.

The system is not, at present, designed to maintain such a large tension in equilibrium. As one can see from the mooring line force response, see Figure 3.8, the tension force in the line at $\epsilon = 5\%$ is $50\ kN$. That is more than twice as much as the maximum lifting force of float number one, which is $18\ kN$. This leads to the conclusion that the floaters have little effect as they will be deeply submerged, and the vertical component of the mooring force on the buoy will be increased with increasing tension. It is therefore likely that the heave response of the buoy is decreased by the increased tension.

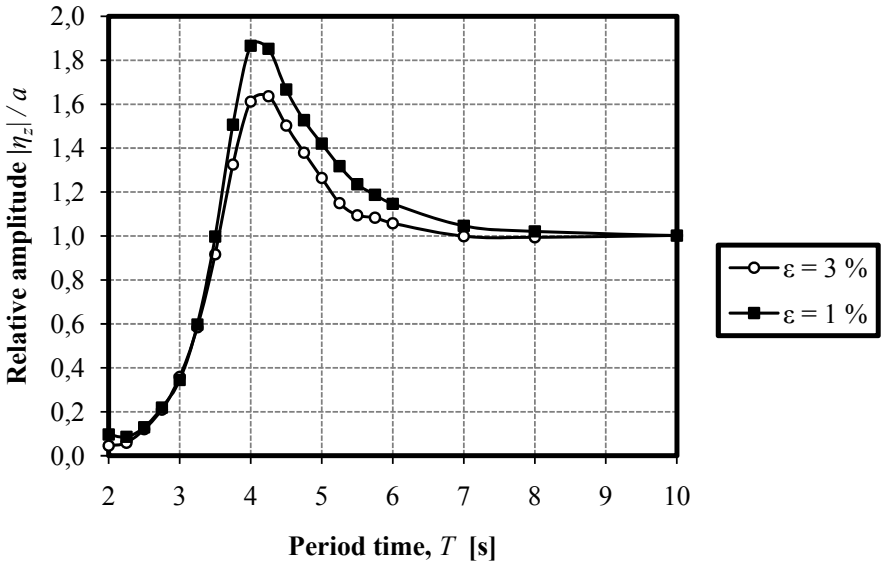

Figure 4.39: The impact of increased pre-tension in the lines on the resulting relative amplitude of the heave motion. All simulations have been made with locked piston configuration.

The increased tension in the lines does affect the heave motion of the buoy in a negative way according to Figure 4.39. It does not however change the eigenperiod of the system, which might have been expected.

The hypothesis that it is the increased vertical tension that produces the drop in heave is now tested by increasing the floater radius by $50\,\%$ whilst maintaining the increased equilibrium strain in line 2 at $\epsilon_2 = 3\,\%$, and doing another sweep over period times. The masses and maximum buoyancy forces of the floaters were also altered accordingly under the assumption that the floater material still had the same thickness and density. The increased bottom surface area of the floater will allow a larger tension force in line number two without the floater being submerged. This will better maintain the horizontality of line number one.

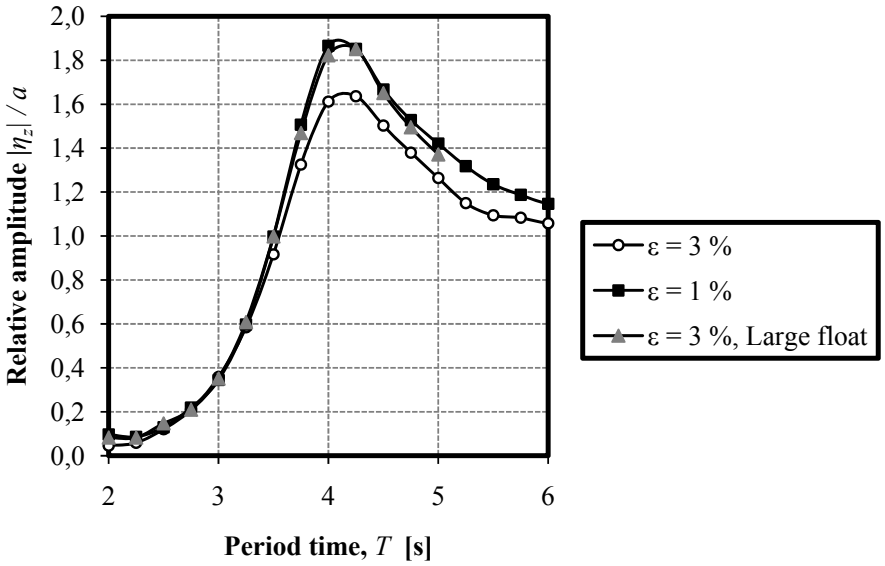

Figure 4.40: The relative amplitude of the buoy heave response as a function of period time. The figure depicts the effect of increased pre-tension in the mooring line and the increased float size.

Figure 4.40 shows how the computer model predicts an increased heave response, without losing the position mooring capabilities seen in Figure 4.38.

4.13.2 Mooring forces

The mooring forces in the lines during the period sweep with $\epsilon_2 = 3\ \%$ can be seen in Figure 4.41.

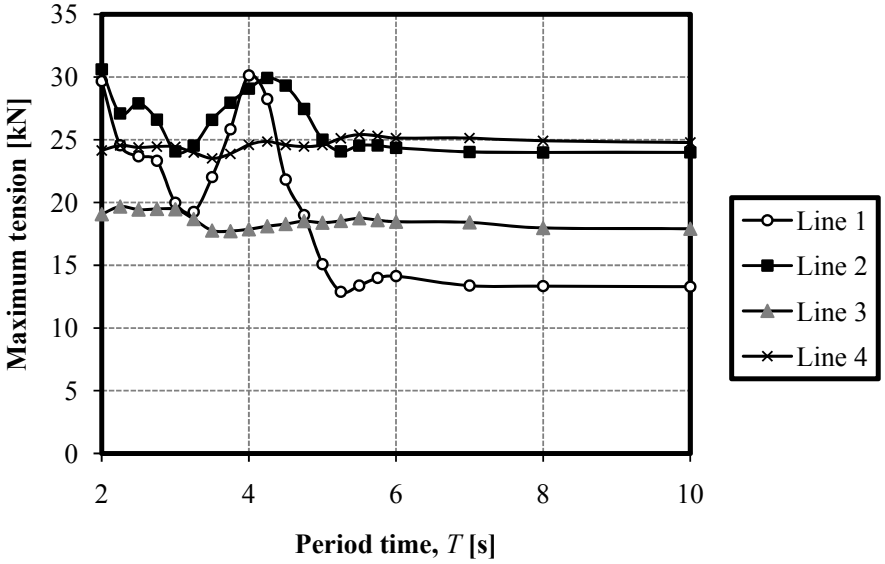

Figure 4.41: The maximum mooring forces as a response to incoming waves of varying period times. The simulation was made with $\epsilon_2 = 0.03$. *This simulation was performed with locked piston.*

The values are generally higher than in Figure 4.21, and they show the same form. However the peak value at resonance remains the same, so that the maximum force in any mooring line is still around $30\ kN$. The buoy response was slightly damped by the increased mooring tension in this simulation. Therefore it is also interesting to look at the force response from the simulation with increased floater size.

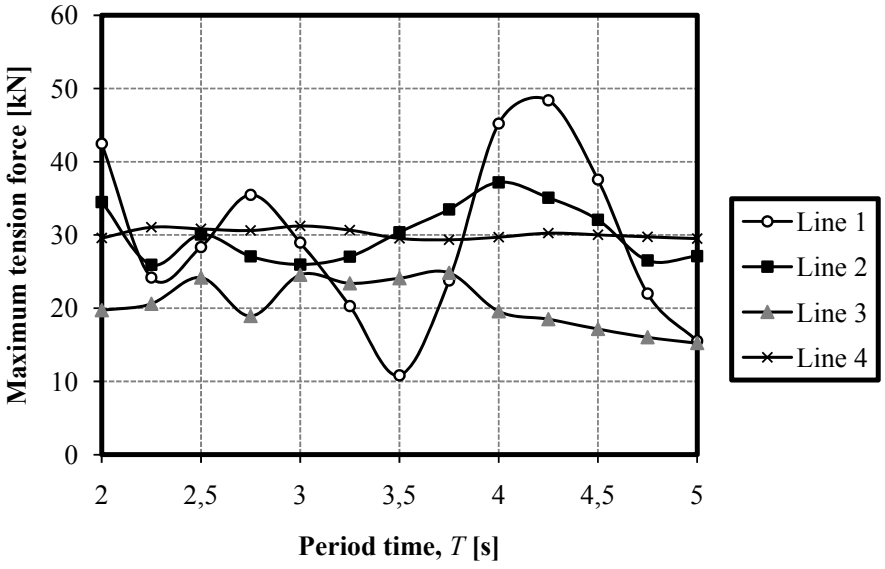

Figure 4.42: The maximum mooring forces of the system with 50 % *increased floater radius, locked piston position and* $\epsilon_2 = 3$ %.

The same form of the curve is seen in Figure 4.42 as in the previous cases, but the entire curve is shifted $10\ kN$ up from Figure 4.41.

The combined results of this section point at how an increased mooring line tension at equilibrium in combination with a suitable floater size can change the properties of the mooring system. The maintained heave motion in combination with the increased positioning capability can, according to my reckoning, be said to compensate for the increased maximum tension force. One must however take care in increasing the floater size too much as this might affect the incoming waves and work as a wave breaker before the buoy is reached by the wave. This has not been taken into account in the simulations and is something that needs to be considered if this alteration of the mooring system is to be taken to the next level.

5 Discussion and Conclusion

The problem of mooring a floating wave power device is, as we have seen, more complicated than it might first appear to be. The results of this thesis shows much of the systematic behaviour of the system, where the effect of changing one parameter individually is studied. This presents a basic understanding of the system and the possible reaction to different loading scenarios. There are many factors that need to be considered and the overall conclusion must be that there are many things left to discover about the behaviour of the mooring system of the WaveEl buoy. This thesis has been focused on the present conditions of the site outside of Vinga and the sizes and lengths of the different components, such as the buoy, the floaters and the lines. The following subsections cover some of the problems and uncertainties that remain to be explored.

5.1 Sources of error and improvements

The computer model that has been constructed during the course of this thesis can of course be improved in a number of ways. There are many assumptions made in the simulations and the effects of some of the major ones are discussed in this subsection.

5.1.1 Buoy assumptions

The behaviour of the buoy is difficult to model exactly as it will change its dynamic properties during operation as the piston will exert a varying force on the buoy. In the simulations only the positions of locked and free piston configuration are considered and a future version might include the simulation of the buoy and the piston as separate rigid body elements with connection forces corresponding to the load of the generator.

The long-wavelength approximation is another uncertainty which comes into play when analyzing the low response in heave for the buoy with free piston. The elevation of the wave is assumed to be constant across the diameter of the body. Only then is the approximation of Morisons formula, which expresses the forces on the body as a function of the relative velocity and acceleration, accurate. In the case of the buoy with free piston at resonance the wavelength is basically of the same size as the diameter so that the resulting forces are somewhat misleading. The use of complete diffraction theory must then be used.

An additional source of error is the constant assumption made about the added mass properties of the buoy. The frequency dependence of the added mass is discarded in the simulations and it would therefore be interesting to investigate its impact on the system. The frequency and velocity dependence of the drag coefficient is taken to be valid throughout the simulation and at all locations independently of position. This is not entirely accurate as the flow close to the surface is significantly more turbulent than the flow at the bottom of the buoy $20\,m$ below. The impact of this is that the simulations of loading cases involving turbulent flow at maximum speed has been

using a slightly lower drag force than would have been the case in a model that takes the position dependence into account.

5.1.2 Floater assumptions

One of the roughest approximations is concerned with the floaters. They are simulated to be vertical cylinders at all times. This is of course not the case, for they will tilt in response to the current and wave loading and their angular displacement will be inversely proportional to the level of submersion. As this tilting effect is not taken into account, the resulting forces will be somewhat too large and they will respond more strongly to the water motion than in reality. As we have seen the motion and velocity of the float is a very important factor in the approximation of the maximum tension force of the horizontal line, so in this respect the line tensions are very conservative. That is the mooring forces of the simulations are larger than they would have been if the floaters had been allowed to rotate. This is the main object of revision when it comes to the programming assumptions, as it might have a large impact on the results.

5.1.3 Mooring line assumptions

The mooring line assumptions are above all sensitive to the resolution. The low resolution used in this thesis implies errors in the assumptions about the straight appearance at all times, the linear shape functions and the lumped mass technique. Especially the shape function linearity is misleading as the wavelength of the incoming waves in many cases is smaller than the length of the horizontal lines. As a consequence the velocity of the water is for instance varying across an entire period whilst the simulation only approximates it to be linear between the buoy and the halfway point, and then linear from the halfway point to the floater. The use of a high-resolution model might be of interest to minimize the effect of these errors.

5.2 Mooring system changes

The idea behind the mooring system of the WaveEl buoy is very good, as it has the potential to fulfil all requirements of a mooring system for wave power devices. It has however in its present form still some drawbacks. The system needs to be more rigid if it is to meet the demands of position mooring in a wave power park. This can be solved to some extent by an increased tension in the mooring lines, but that requires an increased size of the floaters in order to keep the horizontality of line one, three and five. This would ensure the heaving freedom of the buoy, as well as keep it horizontally stable. Another way of setting up the system would be to have a wide and not so high floater form, and allow it to be up to 60 % submerged at equilibrium. The horizontal line could then be fastened on the upper side of the floater so that it truly is horizontal at equilibrium in calm water.

Another problem with the mooring system as it is designed today is the slacking of the line, which is not only a computational problem but also might induce fatigue effects

due to the repeated twitching load. This problem might also be minimized by carefully choosing the size of the floaters and the level of pre-tension in the moorings. Another possible option is to increase the length of the horizontal lines, so that they can encompass a larger relative displacement between the buoy and the floater within their elastic region. This might also help to decrease the effect of the moorings on the heave motion as the vertical component of the mooring force would decrease. The total area taken up by the mooring system of one device would then of course be increased, which is not desirable in a future wave power park setting.

There is a clear advantage in that the horizontal lines are so elastic, for that allows large displacements within the elastic area and slacking might be avoided. The elasticity of the vertical line might however be subject to further investigation. Its primary purpose is to keep the float connected to it as still as possible in the horizontal direction. This can be done with a much stronger line with only a small elastic region, and this solution might be more suitable to meet the demands on the mooring system.

5.3 Future simulation

The next step in the simulation of this problem would be to create a high-resolution model of the buoy that takes all the above mentioned sources of error into consideration. This might mean that it cannot be based on the program language of MATLAB, and that some other and more efficient computation algorithm must be used to increase the speed. This is especially probable if many systematic investigations are to be performed.

There is, to the best of my knowledge, no simulation results or data available for elastic mooring lines used in this context. That, in combination with the unique mooring solution of a taut system has made the validation process very difficult. One future way of validating the results could be to build an equivalent model in the environment of a commercial program, such as OrchinaFlex, specialized in fluid-structure interaction, and compare results from the different simulations.

5.4 Wave power park

Another simulation problem of interest is to look at the response of an entire park, or grid of WaveEl buoys. The mooring system of such a park would be of a similar appearance as that of a single unit, but with the difference that the floaters would be inter-connected by a line with a sinker that acts as a spring. It would then only be moored to the sea floor on the edges of the grid. A simulation of this type would require the effect of the damping of waves and the radiated waves from each unit to be taken into account, as well as all terms considered for a single unit in this thesis. It is in this setting that the mooring system must keep each buoy as stationary as possible as it is not certain how the waves might interfere. A unit might be completely out of phase with its neighbouring buoy or floater and they must not under any circumstances collide.

5.5 Conclusive remarks

Conclusively the mooring system of the WaveEl buoy is good for use in its present state if it is to be used on a single device. There are a number of improvements that can and in some cases will have to be made before it is ready for use on a commercial scale in a wave power park of buoys. The magnitudes of the mooring forces obtained are not in any way near to the breaking load of the mooring lines according to the suppliers information, and the device itself is "unsinkable", so in this sense it is a good, safe option. But it might be worth to study the system in further detail as the mooring system solution as a whole shows great potential in solving the mooring problem for this type of device. It will be exciting to see how the project evolves from here.

Johannes Palm

2010-06-06

6 References

Fitzgerald, J. (2009): *Position Mooring of Wave Energy Converters.* Ph.D. Thesis. Department of Civil and Environmental Engineering, Chalmers University of Technology, Göteborg Sweden, 2009.

Larsson, F. (2009): *Non-linear finite element analysis*. Department of Applied Mechanics, Chalmers University of Technology, Göteborg, Sweden, 2009

Lindahl, J., Sjöberg, A (1983): *Dynamic Analysis of Mooring Cables.* Report Series A:9. Department of Hydraulics, Chalmers University of Technology, Göteborg, Sweden, 1983.

Bergdahl, L. (2009): *Wave-Induced Loads and Ship Motions.* Report No. 2009:1. Department of Civil and Environmental Engineering, Chalmers University of Technology, Göteborg, Sweden, 2009.

Newman, J.N. (1980): *Marine Hydrodynamics.* The MIT Press, Cambridge Massachusetts. 1980.

Andersen, T.L. et. al. (2003): *AquaBuoy; Model tests at Aalborg University*. Department of Civil Engineering, Aalborg University, Denmark, 2003

Gruppen för vågenergiforskning, (1981): *Vågenergiforsking I Sverige, Slutrapport etapp 4. Del IV Teoriutveckling.* Rapport GR:44, Göteborg, Sweden, 1981.

Mårtenson, N. (1988): *Dynamic Analysis of a Moored Wave Energy Buoy*. Report GR:56, Chalmers University of Technology, Göteborg, Sweden, 1988.

Bergdahl, L., Rylander, A. (1980): *Förankringskradftmätningar på ett vågkraftverk I havet.* Rapport GR:38 Göteborg, Sweden 1980

Bergdahl, L., Olsson, G. (1981): *Konstruktioner I havet. Vågkrafter-Rörelser.* Report Series B:25. Department of Hydraulics, Chalmers University of Technology, Göteborg, Sweden, 1981.

Sjöberg, A., Bergdahl, L. (1981): *Förankringar och förankringskrafter.* Report Series B:30. Department of Hydraulics, Chalmers University of Technology, Göteborg, Sweden, 1981

Pascoal, R. et. al. (2005): Assessment of the effect of mooring systems on the horizontal motions with an equivalent force to model. *Ocean Engineering.* No. 33 2006, p. 1644-1668.

Lindahl, J. (1985): *Modellförsök med en förankringskabel.* Report Series A:12. Department of Hydraulics, Chalmers University of Technology, Göteborg, Sweden, 1985.

Liu, Y. (1998): *Dynamics and Extreme Value Problems for Moored Floating Platforms.* Report Series A:29. Department of Hydraulics, Chalmers University of Technology, Göteborg, Sweden, 1998.

Bergdahl, L. (1979): *Beräkning av vågkrafter,* Undervisningsskrift Nr 1979:07. Department of Hydraulics, Chalmers University of Technology, Göteborg, Sweden, 1979.

Lindahl, J. (1981): *Rörelseekvationer för en kabel.* Report Series B:24. Department of Hydraulics, Chalmers University of Technology, Göteborg, Sweden, 1981.

Det Norske Veritas (2000): *Environmental conditions and environmental loads.* Classification notes no. 30.5. Norway, 2000

Wave Dragon (2010): *Personal communication*

Bergdahl, L. (2010): *Personal communication with Lars Bergdahl*

Vattenfall (2010): *Personal communication*